General Control Framework for Shape Memory Alloy Based Actuators

A Phase Transformation Approach

T.J. Koomen

Master of Science Thesis

TU Delft Delft University of Technology

Delft Center for Systems and Control

General Control Framework for Shape Memory Alloy Based Actuators

A Phase Transformation Approach

Master of Science Thesis

For the degree of Master of Science in Mechanical Engineering at Delft University of Technology

T.J. Koomen

June 12, 2015

A15.015.1206

Faculty of Mechanical, Maritime and Materials Engineering (3mE) · Delft University of Technology

Abstract

Shape Memory Alloy (SMA)-based actuators are versatile actuators with a high power-to-weight ratio and they are easy to miniaturize. These actuators are ideal for applications such as smart wings and smart rotors. However, SMA-based actuators are generally difficult to control, due to a low bandwidth and a hysteretic and non-linear response.

A general control framework for SMA-based actuators is proposed. This new control framework deals with some of the challenges that are generally faced when working with SMA-based actuators. The biggest challenge that was set was that there is no information on the some of the states of the SMA actuators, such as the temperature or the stress in the material. The general control framework eliminates the need for this information and also proposes a simple method to control multiple inputs to the actuator based on a single output of the system. The main goal of the general control framework is to provide control with increased bandwidth applicable to all SMA-based actuators with control parameters which are easy to tune.

The general control framework, or *Phase Transformation Approach*, focuses on fundamental properties of the SMA material. By using some of the fundamental properties to construct four control laws, the general control framework ensures that is effective for all SMA-based actuators. The control principles were tested and showed that the proposed control framework was effective. However, the parametrization of the control framework was not straightforward. It seemed to have a strong dependency on the amplitude and frequency of the reference signal, also due to the still non-linear response. The individual control principles were effective at achieving what they were designed for but their hierarchy within the general control framework has to be rearranged.

Contents

List of Figures

List of Tables

Acknowledgements

First I would like to sincerely thank my supervisors for their trust and the interesting discussions that we have had. The idea for the subject for my thesis was suggested by one of my supervisors, Adrián Lara-Quintanilla from the Faculty of Aerospace Engineering (AE) and made possible by my other supervisors Jan-Willem van Wingerden and Sachin Navalkar from my own faculty of Mechanical, Maritime and Materials Engineering (3mE). I have learned a great deal from my graduation project and not only from the theoretical and scientific perspective, but also about the application of the knowledge that I have gained during my master courses to actual systems. The experience once again confirms the words of Einstein: *In theory, theory and practice are the same. In practice, they are not.*

I would also like to thank Kees Slinkman and Will van der Geest, the technical staff of the Delft Center for Systems and Control (DCSC) labs. They were always there to help when I needed equipment or with the implementation of said equipment. If it would not have been for them it would have taken a lot longer to build the set-up.

My thanks also go out to Hans Hellendoorn for accepting to be on my MSc. defense committee alongside my supervisors. Finally I would like to thank many of my fellow students and friends who have either been a there to listen to me rattle on about my theories or for the interesting discussions that we have had.

Delft, University of Technology — Teun J. Koomen
June 12, 2015

"Everything should be made as simple as possible, but not simpler."

— *A. Einstein*

Chapter 1

Introduction

This report presents the research of my MSc thesis project. The aim of the research is to investigate the possibility of a general control framework for a specific type of actuator; the Shape Memory Alloy (SMA)-based actuator.

1-1 Background

Within the field of wind turbines, as well as the field of aeronautics, a significant amount of research has been done on the so called smart rotors and smart wings [1, 2, 3]. Smart wings have the ability to change their shape and thereby change their aerodynamic properties. These smart wings can counteract fatigue loads and thereby extend the lifetime. Extending the lifespan or increasing the maintenance interval will in the end reduce the overall costs for wind turbines.

The lifespan is a very important factor in the design of a wind turbine and it is influenced by many factors. The negative influences of the wind and wind gusts on the lifespan of the wind turbine are minimized as much as possible by optimizing the structural design of the wind turbine. However, the wear can be minimized even further by means of active control. Certain wind speeds or wind gusts can excite structural modes of the turbine blades or of the turbine tower. This excitation can be prevented by actively controlling the aerodynamic loading for each turbine blade. This can either be achieved by individual pitch control of the turbine blades or by changing the camber of the turbine blade. The first option can already be applied since all the required hardware is present in modern wind turbines. However, it leads to a higher wear on the bearings and motors. A better option would be to control the camber of the blades by introducing one or more actuators in each of the turbine blades.

One possible actuator that can be used to manipulate the camber of the turbine blades is an SMA-based actuator[4]. This actuator uses SMA wires that can individually be contracted. This allows for the SMA wires to bend the polymer beam that they are embedded in. The exact working of the actuator will be explained later on. Though the focus is primarily on the application to a turbine blade, the SMA-based actuator could also be applied to a fixed wing aircraft.

1-2 Problem Statement

Although these SMA-based actuators have been researched for over two decades now, they still remain unused in common applications. This is mostly due to that they are not easy to control, since their response is very hysteretic and non-linear.

Most research in to the operation and control of SMA-based actuators is very case specific and a general framework seems to be missing[5]. A lot of problems with the control of SMA actuators are only solved for a specific application, such as controlling the system with a trained Neural Network system. These kind of solutions will most likely not be effective for other SMA-based actuators.

The most important factor for all control principles that will be used in this thesis is that they have to be based on fundamental properties of the SMA material. This is a way to ensure that the control framework will be valid for other SMA-based actuators. Also, further research into the effects of the multi-input control of SMA-based actuators is required. The thesis objective can be summarized as:

> To develop a parameterized control framework for SMA-based actuators which linearizes the response using control laws that are based on fundamental properties of the SMA material.

To review the effectiveness of the general control framework, the following questions are formulated:

1. Can the proposed control framework be parameterized such that it cancels out the hysteretic and non-linear response of the actuator?
2. What is the maximal bandwidth that can be achieved with this control framework with a phase delay smaller than 30 degrees?
3. What is the influence of different initial conditions of the SMA actuators on its performance?

1-3 Methodology

This thesis will really focus on the fundamental properties of the SMA actuator itself. If a fundamental property that hinders the control of the actuator can be identified, a

new control strategy can be devised to counter this. This way, the control strategy will be applicable for all SMA-based actuators as long as the right material properties are used. This research focuses on a system which also uses compressed air to actively cool the actuator, whereas most systems only use active heating. The introduction of the two air inputs to the system not only complicates the modeling of the subsystems, but it also complicates the control of the actuator since the air exerts a force from within the actuator.

A portion of the research focuses on the deployment of the hardware that is used to control and power the SMA-based actuator. A new setup was constructed and its performance will shortly be discussed. The goal is to construct a control framework with a low level computational requirement. When the control algorithm is not computationally intensive it is easy to combine multiple SMA-based actuator modules to form larger wing surfaces of which the modules can individually be controlled.

The performance of the general control framework is tested for use with a SMA-based actuator. The performance is reviewed for each of the challenges that are generally faced during controller design for an SMA-based actuator.

1-4 Outline

Chapter 2 elaborates on the principles of the SMA material and their application as SMA actuators. Then the design and principles of the SMA-based actuator as designed by my supervisor are discussed. Chapter 2 looks at some of the mechanics and modeling methods of the SMA-based actuator. In Chapter 3, the challenges of controlling these SMA-based actuators are briefly discussed and a proposal for a new control strategy based on theory as discussed in Chapter 2 is made. In Chapter 4 the proposed control strategy will be tested and compared to other control strategies. This thesis concludes with conclusions and recommendations in Chapter 5.

Appendix A contains detailed specifications of the hardware that was used for the experiments. Appendix B contains more information on the results from the parameterization of the control framework from the experiments. It also lists the best and worst performing parameters for the control framework that were encountered during the experiments.

Part I

Theory

Chapter 2

Shape Memory Alloy

Shape Memory Alloy (SMA) is an alloy which exhibits very distinctive behavior when it is deformed and then heated. In order to obtain a proper understanding of the behavior of SMA, the properties of this material will first be discussed. Once the material properties have been discussed, the modeling methods that are relevant for this thesis work are reviewed. At the end of this chapter, the knowledge of the SMA material and the modeling methods will be applied to the SMA-based actuator. This will allow for a better understanding of its operation and control challenges.

2-1 SMA properties

SMA exhibits a solid-state phase transformations when it goes through a specific temperature cycle. The phase transformations and corresponding crystalline structures that present themselves in the different stages of the cycle are depicted in Figure 2-1. When the material is heated to a certain temperature, which depends on the internal stress, a phase transformation is triggered. During this phase transformation the crystalline structure of the material completeley changes. For a wire made of SMA it means that it will contract. If the material has been deformed beforehand, this process is capable of recovering the material to its original shape. This phenomenon is called the Shape Memory Effect (SME).

Shape Memory Effect

The SME cycle consists of two phase transformations; the *forward transformation* when the SMA is cooled and the *reverse transformation* when the SMA is heated. The graph in Figure 2-2 shows the full SME cycle for SMA material which has no initial stress

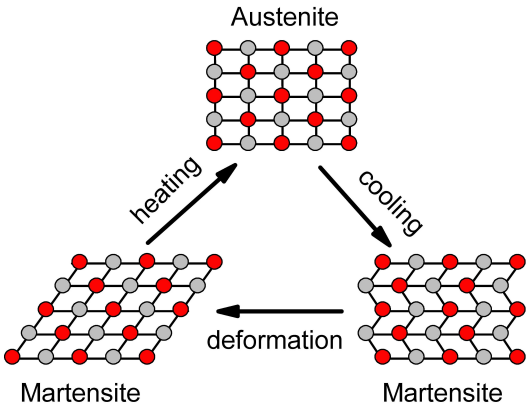

Figure 2-1: Illustration of different phase transformations of the SMA in the Shape Memory Effect cycle (source: Creative Commons (CC)). Bottom left corner depicts the detwinned martensite and the bottom right depicts the twinned martensite

and an initial temperature of zero degree Celsius. The material starts in point B when a force is applied to the material, which causes stress and strain to develop in the material, following the curve in the graph from point B to point C. The twinned martensite has now been transformed into detwinned martensite, which has the same cubic system structure, but the molecules have been rearranged. The load is now removed from the material, causing the stress to drop from point C to point D in the graph. Though the force is removed, the strain remains present in the material. When the detwinned martensite is heated to a certain temperature, a solid state phase change occurs where the crystalline structure changes into an austenite structure. During this transformation, the material recovers its original shape. As the SMA cools down to zero degrees Celsius, another solid state phase change occurs and the material is transformed into twinned martensite crystalline structure again. The forward transformation is an exothermic process, thus it causes the SMA wire to develop some heat during the cooling process [6].

This remarkable feature of the SMA is that this cycle can be repeated many times, as much as ten million times depending on the specific SMA material, the continuous stress that the SMA material is subjected to and the recovered strain [7]. The maximum recoverable strain typically lies somewhere in the range of 5% to 8%, which is high for metal alloys. The expected lifetime of the wires used for this thesis is depicted in Figure 2-3, where it is clear to see that high levels of strain and stress reduce the expected number of lifecycles of the SMA material.

SMA temperatures

The phase transformations of the material are triggered when certain temperatures are reached. These temperatures depend on the stress level in the material; the higher the stress, the higher the temperature needs to be. This stress and temperature correlation

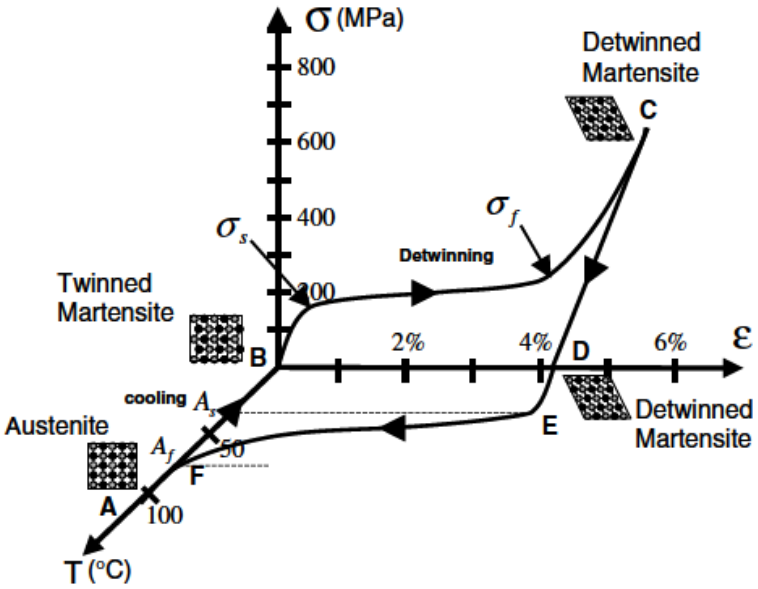

Figure 2-2: Graph depicting the SME cycle and corresponding stress, strain and temperature

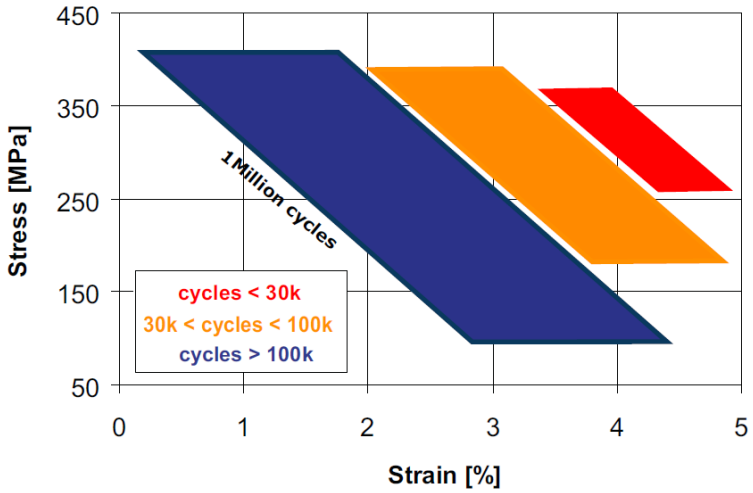

Figure 2-3: Expected number of life cycles as a function of stress and strain during cycles (© SEAS Getters).

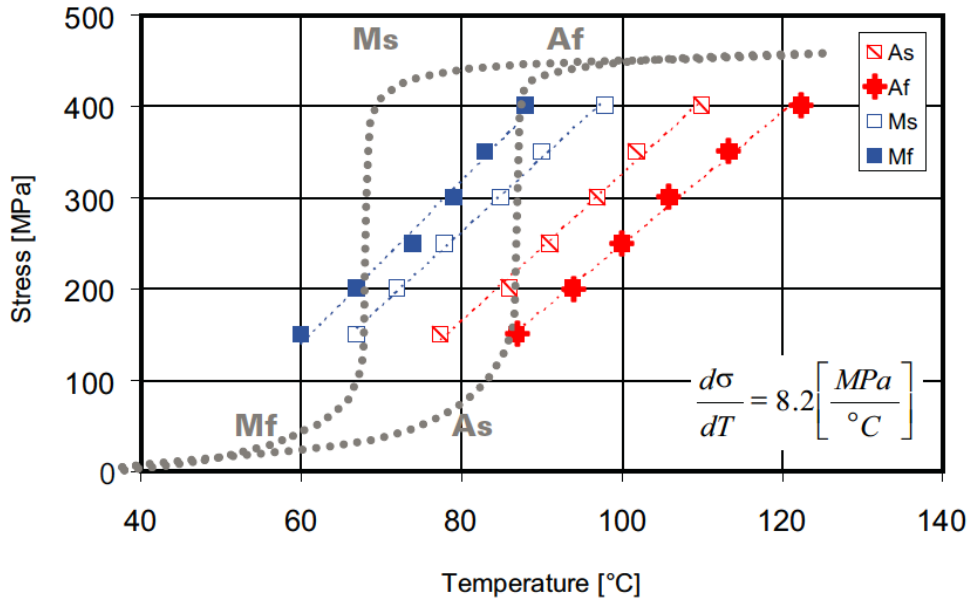

Figure 2-4: Transformation temperatures for SMA wires as a function of the internal stress. The dotted line is an example of the strain during a SME cycle for an SMA wire. The dots from the legend that are connected by the small dotted lines indicate the respective starting or finishing temperatures for the different transformations for different stress levels. (source: SAES Getters)

is depicted in Figure 2-4. There are four important transformation temperatures for the SMA material, namely the temperatures for martensite finish M_f, martensite start M_s, austenite start A_S and austenite finish A_f. They indicate the temperature where the transformations start or finish. The grey dotted line in the figure depicts the process for a wire with a *constant* stress of approximately 150 MPa. The colored dots in the graph indicate the different temperatures for the starting and finishing points for varying internal stress. From this graph, it already becomes clear that both temperature and stress play a significant role when determining the phase of the material. Therefore these factors are also really important in determining the amount of deformation of the SMA material. The graph in Figure 2-4 can basically be summarized into 3 regions:

$$\begin{array}{llll} \text{Region } I: & & T < M_s(\sigma) & \rightarrow \text{Forward transformation of SMA} \\ \text{Region } II: & M_s(\sigma) < & T < A_s(\sigma) & \rightarrow \text{No transformation of SMA} \\ \text{Region } III: & A_s(\sigma) < & T & \rightarrow \text{Reverse transformation of SMA} \end{array} \tag{2-1}$$

2-2 Modeling SMAs

Modeling of SMA is not straightforward due to the presence of three different crystalline phases in the material at different stages during the SME cycle [8]. Because the phase changes during the SMA cycle, the material properties are *discontinuous*. A property like the convective heat transfer coefficient h is dependent on the phase as well as the temperature [9, 10]. As a results of this, some of the properties of the SMA wire are governed by discontinuous functions. In this section two constitutive modeling methods will be discussed; the first one is based on a thermodynamical approach and the second one is a more mechanical approach. These two approaches are the two main model types found in literature that are used to describe the behavior of SMA material .

2-2-1 Thermodynamical approach

The constitutive model, or free-energy model, tries to resolve the difficulties of modeling by combining the properties of the three phase fractions into a single model [11, 12, 13]. Three phase fractions x_{M+}, x_{M-} and x_A are introduced, which are governed by the evolution of the martensitic fractions ((2-2) and (2-3)). Since the sum of fractions needs to equal one, the austenite phase fraction can be written as (2-4).

$$\dot{x}_{M+}(t) = -p_{+A}x_{M+}(t) + p_{A+}x_A(t) \tag{2-2}$$
$$\dot{x}_{M-}(t) = -p_{-A}x_{M-}(t) + p_{A-}x_A(t) \tag{2-3}$$
$$x_A(t) = 1 - x_{M+}(t) - x_{M-}(t) \tag{2-4}$$

Here x_A is the austenite phase fraction, x_{M+} is the tension-induced martensitic phase faction, x_{M-} is the compression-induced martensitic phase fraction and p_{ij} are the phase transition probabilities. Since an SMA wire can only experience tension forces it is assumed that at low temperatures the material is composed of detwinned martensite (M_+) at high stresses and twinned martensite ($M_{+/-}$, which is a blend of both martensite phases) at low stress.

The phase transition probabilities are determined by examining the barriers in the Gibb's energy landscape. The exact details on this can be found in the Phd dissertation by Heintze [14]. The non-linear stress-strain relation for an SMA tendon is given by:

$$\sigma(t) = \frac{\varepsilon(t) - \varepsilon_T(x_{M+}(t) - x_{M-}(t))}{\frac{x_A(t)}{E_A} + \frac{x_{M+}(t)+x_{M-}(t)}{E_M}} \tag{2-5}$$

Here $\varepsilon(t)$ is the strain of the SMA wire, ε_T is the transformation induced strain, E_A is the Young's modulus of the austenite phase and E_M is the Young's modulus of the martensite phases. Equation (2-5) divides the strain which is not a direct result of the

transformation, by a phase fraction dependent elasticity modulus to yield the stress in the SMA. The thermodynamic behavior of the SMA is described by

$$\underbrace{mc\dot{T}(t)}_{\substack{\text{Energy}\\\text{flux}}} = \underbrace{-hA_s(T(t)-T_\infty)}_{\substack{\text{Energy dissipation by}\\\text{(natural) convection}}} + \underbrace{H\dot{x}_{M+}(t)+H\dot{x}_{M-}(t)}_{\substack{\text{Latent heat from}\\\text{transformations}}} + \underbrace{j(t)}_{\substack{\text{Heat}\\\text{input}}} \tag{2-6}$$

Here m is the mass of the SMA wire, c is the specific heat capacity, h is the convective heat transfer coefficient between the SMA wire and ambient air at temperature T_∞, A_s is the surface of the SMA wire, H is the latent heat of phase transformation and $j(t)$ is the Joule heating input. Equation (2-2) to (2-6) together describe the constitutive behavior of a SMA wire.

2-2-2 Mechanical approach

The other approach that is considered is that of Arai et al. [15] with the improvement made by Wang and Yan [16]. This model is derived from a more mechanical than thermodynamic perspective and describes the relationship between the temperature to the development of strain and stress in the SMA wire. It achieves this by first looking at the mechanical energy per unit length of the wire (2-7), where c_0, c_1, c_2 and c^* are constants, T is the temperature of the wire and ε is the strain of the wire.

$$U = c_0 + \frac{1}{2}\varepsilon^2 + \frac{1}{4}c_2\varepsilon^4 - c^*T\varepsilon \tag{2-7}$$

According to the relationship (2-8), where c is defined by the current phase state of the SMA, the generalized temperature $(T - c\sigma)$ can be used instead of T to describe the stress dependence of the transformation temperatures. A viscous coefficient γ is introduced, which will account for the viscous damping which occurs during the phase transformations. Equation (2-9) represents the relation between the elastic and the viscous force of the SMA.

$$\frac{\partial\sigma}{\partial T} = \frac{1}{c} \tag{2-8}$$

$$\frac{\partial U}{\partial\varepsilon} + \gamma\dot{\varepsilon} = 0 \tag{2-9}$$

Combining Equations (2-7) through (2-9) yields the generalized formula as in (2-10), where the origin (T_0, ε_0) can be chosen at any place

$$\hat{\gamma}\dot{\varepsilon} + \hat{c}_1(\varepsilon-\varepsilon_0) + \hat{c}_2(\varepsilon-\varepsilon_0)^3 = T - T_\infty - c\sigma \tag{2-10}$$

Wang and Yan [16] adapted this formula in such a way that it can also describe the hysteresis curve of the SMA. Hence, the previous formula mainly focuses on the strain and temperature relation, and not the stress-strain. A non-elastic term is added to (2-10), which contains a certain error function as defined in (2-12). The error function is active in both the loading and the unloading phase of the SMA cycle, which allows for more accurate modeling of the super-elastic hysteresis curve of the SMA.

$$\hat{\gamma}\dot{\varepsilon} + \hat{c}_1(\varepsilon - \varepsilon_0) + \hat{c}_2(\varepsilon - \varepsilon_0)^3 = T - T_\infty - c\left[\sigma - \hat{c}_3\left(\sigma - \sigma_0\right)^{\hat{c}_4} f_{\text{err}}\left(a\left(\sigma - \sigma_0\right)\right)\sigma_0\right] \quad (2\text{-}11)$$

$$f_{\text{err}} = \frac{2}{\sqrt{\pi}} \int_0^x e^{-t^2} \mathrm{d}t \quad (2\text{-}12)$$

A special case arises according to Wang and Yan [16] when ε and $\dot{\varepsilon}$ are equal to zero (ε_0 *can* take any positive value). In that particular case, the stress that develops in the wire is defined by (2-13), where c is a constant of the SMA.

$$c(\sigma - \sigma_0) = T - T_\infty \quad (2\text{-}13)$$

Given the fact that the stress that develops in the wire when the phase transformation is triggered actually causes the austenite starting temperature A_s to increase, then it might results in a (piece-wise) linear relation. However, no proof was found that this will be the case for the SMA actuators that were used this thesis work, since both the strain ε and the strain rate $\dot{\varepsilon}$ will not exactly be equal to zero. This property of SMA material will be reviewed in Chapter 3.

2-3 SMA actuator

SMAs in the form of wires, springs or beams are also often referred to as SMA actuator whenever it is used to deliver a force or displacement. SMA actuators have the highest power-to-weight ratio among light-weight actuation technologies [17, 18]. This makes it an ideal actuator for miniaturization or applications where the actuators needs to be integrated, or retrofitted, into an existing design. The SMA actuator is an ideal actuator for situations where miniaturization or clean and silent operation is required.

These SMA actuators can be applied in many ways, but the most general one is as a muscle-like actuator. An example is depicted in Figure 2-5, where an SMA wire is subjected to a constant load from a mass with weight m. Due to the mass, the SMA wire has been elongated by length change dL. When the circuit closes and a current passes through the SMA actuator it heats up. As the temperature of the wire reaches A_s, it starts to transform into the austenite crystalline structure which causes the wire to contract. the transformation is complete when the entire wire is heated to a temperature

of A_f. At this point, the wire has contracted a length of dL. When the circuit is opened again, the wire slowly cools down. When the temperature of the wire reaches M_s, it slowly starts to elongate again due to the mass that is suspended from the wire. When the temperatures passes M_f the transformation is complete and the wire has returned to its previous length L_0.

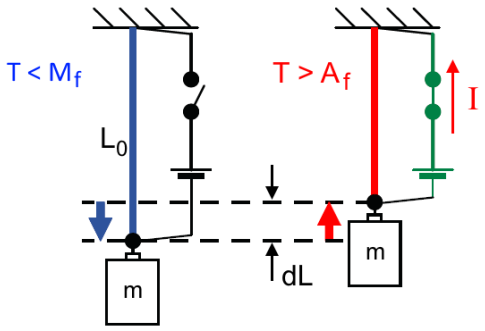

Figure 2-5: Example of the use of an SMA actuator subjected to a constant load.

2-3-1 Functional Fatigue

Functional fatigue is a phenomenon which occurs during the first several thousand life-cycles of new wires. The SMA material slowly develops a permanent elongation (strain) which is unrecoverable and the maximum recoverable strain decreases. The permanent elongation is approximately 0.2 percent after 50.000 cycles for the type of wire that is used in the SMA-based actuator [19]. The effect of the functional fatigue becomes apparent when the responses of a new wire and a wire that has been subjected to 5000 full cycles is plotted in Figure 2-6. The initial full stroke for the new wire is 5.8 %. After it has been cycled 5000 times, a full stroke of 5.2 % remains. The cycling effects the micro structural features and the actuation performance of the actuator.

This response degradation and development of permanent elongation does not continue through the entire lifespan of an SMA actuator. Eventually, after a number of cycles, which ranges from 10.000 to 60.000, the behavior of the actuator converges [19]. It is deemed sufficient that SMA wires are used that have been conditioned in order to ensure consistent results. No further attempt was made to incorporate the response degradation of the SMA actuator in the modeling methods as it would hardly improve the functionality of the SMA actuator.

2-3-2 Modeling of SMA temperature

The temperature of an SMA wire itself can best be modeled by the simple equation (2-14).

$$\frac{dT}{dt} = \frac{\dot{Q}_{\text{in}} - \dot{Q}_{\text{out}}}{m\, c_p} \tag{2-14}$$

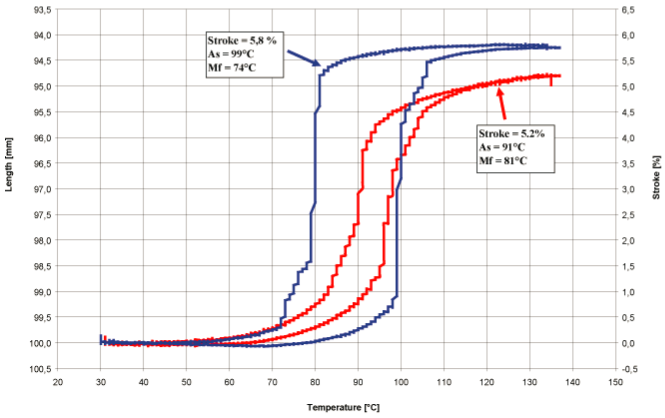

Figure 2-6: Response for a new SMA wire and an SMA wire that has been subjected to 5000 full cycles (source: SAES Getters)

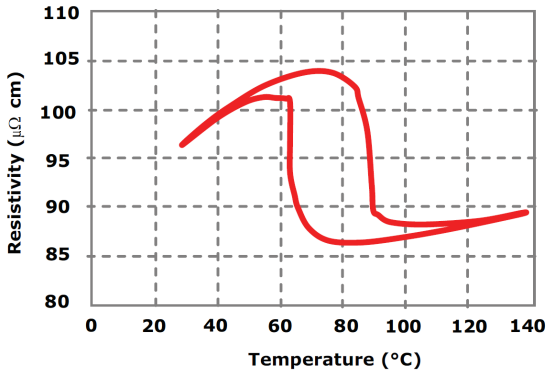

Figure 2-7: Resistivity of SMA material (source: SAES Getters)

The terms $\dot{Q}_{\text{in}}$ and $\dot{Q}_{\text{out}}$ are defined by (2-15) and (2-16), where I is the current through the SMA wire, R_{SMA} is the resistivity for the SMA material and $h(F_i)$ is the convective heat transfer coefficient as a function of the valve aperture i. The convective heat transfer coefficient is almost linear in the valve aperture, but the resistance of the wire is a non-linear function of the temperature and the phase of the SMA (Figure 2-7). The function for the resistance also show a similar hysteresis loop as the description for the phase transformation of the SMA.

$$\dot{Q}_{\text{in}} = I^2 R = I^2 R_{\text{SMA}}\left(T\left(t\right)\right) \frac{L}{A_{\text{SMA}}} \tag{2-15}$$

$$\dot{Q}_{\text{out}} = A_{\text{conv}}\, h\left(F\right)\left(T\left(t\right) - T_{\infty}\right) \tag{2-16}$$

The temperature response of the SMA wire can be defined as (2-17), where the latent heat that develops during the cooling process has been neglected. The temperature

response of the SMA will behave like a damped system. At $t = 0$ when a current is sent through the SMA wire, the term $\dot{Q}_{\text{in}}$ will drastically increase while the term $\dot{Q}_{\text{out}}$ will only slowly increase as the temperature $T(t)$ rises. At a certain time, $\dot{Q}_{\text{out}}$ will approach the value of $\dot{Q}_{\text{in}}$ and the equilibrium temperature T_{eq} will be reached. An interesting thing to observe is that both the terms $\dot{Q}_{\text{in}}$ and $\dot{Q}_{\text{in}}$, and the term preceding the integral sign contain the length L of the SMA wire. These terms cancel each other out which implies that the temperature of the SMA wire as a function of I and F is *independent* of its length.

$$T(t) = \frac{1}{A_{\text{SMA}} L\, \rho\, c_p} \int_0^t \left[I^2 R_{\text{SMA}}\left(T\left(t\right)\right) \frac{L}{A_{\text{SMA}}} - \pi d L\, h\left(F\right)\left(T\left(t\right) - T_\infty\right) \right] \mathrm{d}t \tag{2-17}$$

Equation (2-17) will be very difficult to solve analytically since it contains a number of discontinuous and/or non-linear terms. Therefore, a description for the equilibrium temperature as function of a constant I and F is defined in (2-18), where $t \to \infty$. This description will be used for control purposes in Chapter 3.

$$T_{\text{eq}} = \lim_{t \to \infty} T(I, F) \tag{2-18}$$

2-4 SMA-based actuators

SMA-based actuators are actuators which use one or multiple SMA actuators in the form of wires, springs or even beams [20] in order to achieve actuation. The SMA-based actuator that is used for this thesis work is depicted in a sketch in Figure 2-8a. It shows the side view of the actuator where the tip of the actuator can deflect in an upwards or downwards motion, corresponding to a positive or negative x direction. The beam in which the wires are placed is made out of a flexible nylon polymer, allowing for deflection of the beam at reasonably low stress levels in the wire. A cross section of the beam is shown Figure 2-8b, where the dashed line indicates the neutral axis of the beam.

The wires that are used in the actuator have been prestrained to 4 % and are then clamped in the actuator under tension. This means that the wires have an initial stress of σ_0 and an initial strain of $\epsilon_0 \approx 4\%$. When the wire is heated to at least the corresponding A_s it will start to transform into the austenite crystalline structure, causing it to recover the initial strain. Contraction of the wire is very limited since it has been clamped in the actuator. Since contraction is very limited, the tension in the wire increases as the phase transformation progresses. In Figure 2-9a and Figure 2-9b the extra tension in the dotted wire, which is heated, causes the beam to bend. This deflection of the tip of the actuator is enhanced when the other wire, the solid wire, is cooled to a temperature below M_s or preferably M_f. This causes the wire to return to the martensite phase

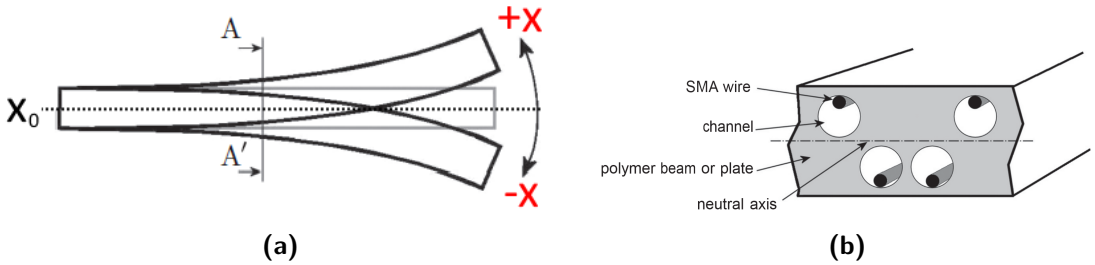

Figure 2-8: Schematic representation of the SMA-based actuator, with **(a)** showing neutral axis x_0 and the deflection in positive and negative x direction and **(b)** the cross section showing the air channels and SMA wires.

and maximize strain and minimize stress in that wire. So when the upper wire of the actuator is heated and the lower wire is cooled as in Figure 2-9a the actuator will exhibit an upward deflection. When the heating and cooling of the wires is switched the actuator will bend downwards as in Figure 2-9b.

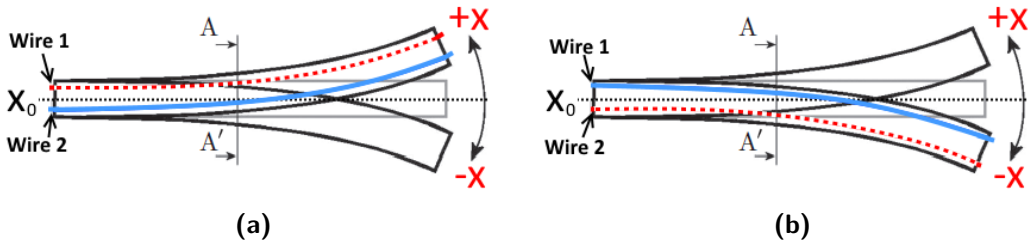

Figure 2-9: SMA-based actuator showing an **(a)** upwards and **(b)** downwards deflection. A dotted wire indicates the heating of the wire, which causes it to contract. A solid wire indicates the cooling of the wire, causing it to elongate.

Inputs and Outputs

From a control perspective, the SMA-based actuator has four inputs; separate heating and cooling control for two wires. The heating is achieved through Joule heating and the cooling by convective heat transfer which can be controlled by increasing the air-flow through the air channels which house the SMA wires. Joule heating is the simple principle of a current I that passes through a wire with a resistance R, which causes the wire to heat up. Most SMA-based actuators only use active heating of the SMA wire or spring. This actuator however, also uses active cooling control by means of compressed air that is fed through the channels that house the SMA wire. The advantage of also actively controlling the cooling process of the SME cycle is that the cooling of the SMA takes significantly longer than the heating of the wire. Thus by increasing the rate of cooling, the speed and hence the bandwidth of the actuator can potentially be increased . The four inputs are defined as in Table 2-1, where the first two inputs are the currents

in amperes and the last two inputs are the valve apertures where zero indicates a fully closed and 1 indicates a fully opened valve. It is important to remark that all inputs have a minimum of zero, i.e. the inputs are always greater or equal than zero and can thus not be negative.

Table 2-1: Four inputs of the SMA-based actuator

Input Designation	Symbol	Unit	Range
Current	I_1	Ampere	<0,20>
	I_2	Ampere	<0,20>
Valve aperture	F_1	(-)	<0,1>
	F_2	(-)	<0,1>

The only output of the system is an external signal measuring the deflection at the tip of the actuator. This measurement is obtained from a laser displacement sensor. At any given time, the stress in both wires and the exact temperature of the wires are unknown. This complicates the use of the modeling methods since they are primarily based on the SMA's temperature and stress. The input is defined as (2-19), where the range of the laser sensor is $[1, 5]$ Volts, which translates to a distance of $[20, 40]$ millimeters from the laser sensor itself. The output of the laser sensor is shown in millimeters and the starting position will always be marked as $\mathrm{x} = \mathrm{x}_0 = 0$.

$$\mathrm{x}\ (\mathrm{mm}) \tag{2-19}$$

2-4-1 Modeling of the SMA-based actuator

The modeling methods described in Section 2-2 only describe the behavior of the individual SMA actuators. A model needs to be conceived to be able to predict the influence of these individual actuators to the SMA-based actuator. Modeling of the SMA-based actuator that is used for this thesis work can best be approached by considering a beam with two wires that are under a certain stress σ_1 and σ_2. The stress will cause the actuator to compress in longitudinal direction, proportional to the Young's modulus of the nylon polymer. The difference in stress between the two wires can be rewritten to a resulting torque at the end of the actuator. The resulting torque M can be used to calculate a deflection at the tip of the actuator. This superposition principle is depicted in Figure 2-10.

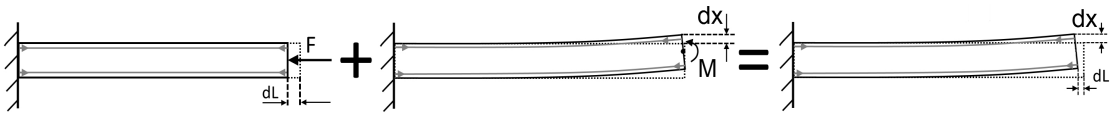

Figure 2-10: Modeling approach for SMA-based actuator using superposition principle

The compression dL of the beam is neglected since it has no influence on the deflection dx and this is the only deformation that we are interested in. The deflection of the tip of the actuator is defined by (2-20).

$$\mathrm{dx} = \frac{ML^2}{2EI} \tag{2-20}$$

$$M = 2\,\alpha\,A_{\mathrm{SMA}}\,(\sigma_1 - \sigma_2) \tag{2-21}$$

Here L is the length of the beam, E is the Young's modulus of the nylon polymer and I is the moment of inertia of the beam. The torque is defined by (2-21), where α is the distance from the wire to the neutral axis of the actuator, A_{SMA} is the surface of the cross section of the wire. The factor 2 in (2-21) is due to the fact that the wires run back and forth over the length of the actuator per side. Therefore the effective number of wires per side is two, thus twice the force. Using Equation (2-13), rewritten as (2-22), and the assumption that the strain is equal to zero, one could consider the response of the actuator to be linear. This will only be possible when the parameter c describing the relation between the temperature and stress is linear and that it is feasible to keep the two wires at constant temperatures. Equation (2-20) can then be rewritten as (2-23). Since the initial stress is assumed to be equal in both wires and T_∞ is also equal for both wires the equation can be reduced to (2-24) where it is clear to see that the deflection is linear in the difference in temperatures of the wires.

$$\sigma_i = \frac{T_i - T_\infty}{c} \tag{2-22}$$

$$\mathrm{dx} = \frac{2\,\alpha\,A_{\mathrm{SMA}}\left(\left(\frac{T_1 - T_\infty}{c} + \sigma_0\right) - \left(\frac{T_2 - T_\infty}{c} + \sigma_0\right)\right)L^2}{2EI} \tag{2-23}$$

$$\mathrm{dx} = \frac{2\,\alpha\,A_{\mathrm{SMA}}\,(T_1 - T_2)\,L^2}{2EI\,c} \tag{2-24}$$

2-4-2 Model Choice

Two modeling methods have been discussed in Section 2-2; the first method with the thermodynamical approach and the second method with a mechanical approach. Both models predict the behavior of the SMA material as a function of the temperature. Unfortunately, these models are not very useful for controlling the actuator since the exact temperatures of the SMA actuators are unknown. The model for the temperature of the SMA actuators can only model the ideal equilibrium temperature and it fails to predict the erratic temperature fluctuations which occur as can be seen in Figure 2-11. Extensive identification for six different data sets have been performed in an attempt to find parameters which could accurately describe the temperature response as a function

of the current I and the valve aperture F. Unfortunately they have not been successful in simulating the erratic temperature fluctuations.

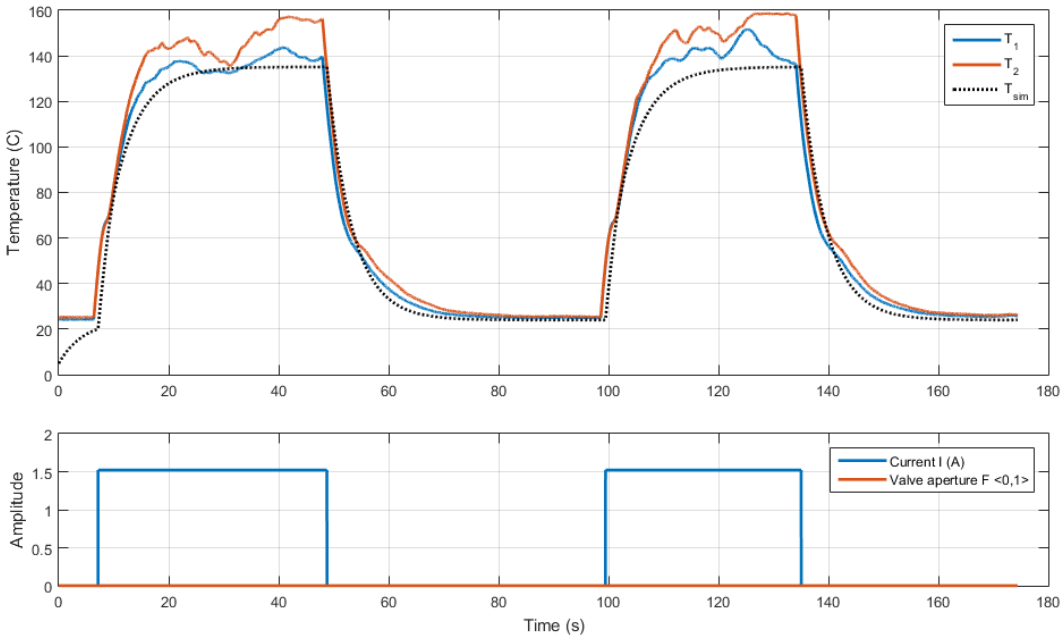

Figure 2-11: Temperature response of a single SMA actuator measured at two points (solid lines; T_1 and T_2) and the simulated *minimum* temperature response (dotted line) for a constant current of 1.5 amperes being switched on and off.

Another interesting observation from Figure 2-11 is that the temperature for the second heating process is slightly higher on average. This is due to the slow heating of the SMA actuator housing. This heating also complicates modeling of the SMA-based actuator and could serve as a motivation to use model free control strategies. However, when the specific heat capacity c_p is correctly identified the temperature models are able to provide an accurate estimate for the *minimum* temperature of the SMA actuator. The presence of reverse transformation in the SMA material can then be ensured if that minimum temperature exceeds $A_s(\sigma_0)$.

2-5 Summary

SMA actuators have some very promising advantages such as the high power to weight ratio. Unfortunately they also suffer from a few disadvantages, such as the hysteresis in the SME cycle. However, if these disadvantages can be overcome, the SMA actuator will be very useful for many applications such as smart rotors for wind turbines. Their

small size and the ability to be shaped into almost any possible shape makes them very versatile.

The modeling methods for the SMAs that were discussed seemed to be able to yield useful information for control design purposes. Unfortunately since the temperatures of the SMA actuators in the SMA-based actuator are unknown the models lose their usefulness. The temperature model can still provide a *minimum* equilibrium temperature for a certain current and valve aperture, which is going to be an important piece of information for solving the hysteresis challenge in Chapter 3. The stress-temperature relation (2-13) from the mechanical modeling approach plays a vital role in attaining a constant stress in the SMA actuators in order to keep the SMA-based actuator at a fixed deflection.

Control strategies have to be pursued that do not employ models that require knowledge on the exact temperature of the SMA actuators. However, the temperature cannot simply be dismissed since the temperature governs the behavior of the SMA. Instead of focusing on an exact temperature, the focus needs to be on a temperature region. To be more precise it has to focus on the phase transformation temperature regions since these regions dictate how the SMA actuators respond.

Chapter 3

Control

This chapter investigates the challenges that are generally faced when designing controllers for Shape Memory Alloy (SMA)-based actuators. After these problems have been discussed, the requirements for a general control framework for SMA-based actuators are established. A short review is then be presented on state-of-the-art control strategies that have been applied to similar actuators. Then the proposal for the new general control framework is introduced. Section 3-5 addresses the control principles that are used in the new control framework and show how they have been established. This chapter is concluded with a summary.

3-1 Problems with SMA control

This section discusses the problems that are generally encountered when working with an SMA actuator. Four challenges are faced with the use of SMA-based actuators:

- Low bandwidth
- Hysteresis
- Non-linear response
- Multi Input, Single Output (MISO) system

The last mentioned challenge is an important factor for the general control framework since the extra inputs are required to increase the bandwidth of the actuator [21]. In the next four paragraphs all challenges of the SMA-(based) actuators are presented.

Low Bandwidth One of the disadvantagess of the SMA actuator is that it has a low bandwidth. This means that the response of the actuator is slow and it will not be able to accurately track a reference that changes rapidly. The actuator behaves like an overdamped system, i.e. a system with a damping coefficient ζ greater than 1. The Bode plot in Figure 3-1 depicts the frequency response of the SMA actuator. In literature it was found that many actuators, of which only one uses active cooling, have a bandwidth which does not exceed 1 Hz [17, 4, 22, 23, 24]. For many applications this bandwidth is not sufficient and therefore, increasing the bandwidth will need to be addressed by the control framework. The desired actuation bandwidth for wind turbine applications of the SMA-based actuator would be 12 Hz [2]. This frequency would be required if the actuator needs to compensate for all of the structural modes of the wind turbine. If only the first mode has to be addressed, 2 Hz will suffice [2].

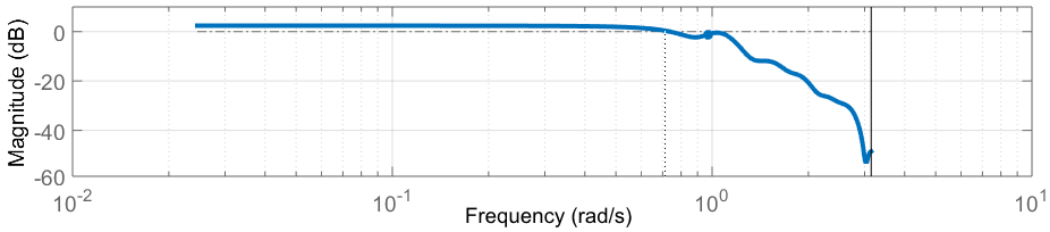

Figure 3-1: Bode plot of SMA actuator

Hysteresis Another disadvantage of the SMA-based actuator is that its behavior is hysteretic. For the actuator to respond, it requires a certain threshold value to be exceeded on the input. This is true for the reverse transformation. The forward transformation can occur as long as the temperature is below M_s, so even when all inputs are equal to zero. The required threshold value can be related to the phase transformation temperatures (2-4). The exact threshold value also depends on the direction of the process, so in the case of an SMA actuator it is different for the forward and reverse transformation. This results in a hysteresis loop, which is visible in the graph in Figure 2-6, where the actuator barely responds until a certain temperature is reached. Ideally, an actuator responds as soon as an input is activated.

Non-Linearity The actuator also has a non-linear response, which is depicted in Figure 3-2. This non-linear response could be accredited to the Joule heating term $\dot{Q}_{\text{in}}$ which is non-linear in the current I_i or the resistance of the wire which is non-linear in the temperature. The graph in Figure 3-3 shows the response of the temperature, measured at two positions, to a constant current being switched on an off. It is clear to see that the temperature shows some erratic fluctuations once it approaches the steady state, or equilibrium, temperature. This could be caused by numerous reasons; heating of the actuator encasing, accuracy of the sensor, phase transformations in the SMA etc. It is logical to assume that, if the temperature is not constant the phase transformation

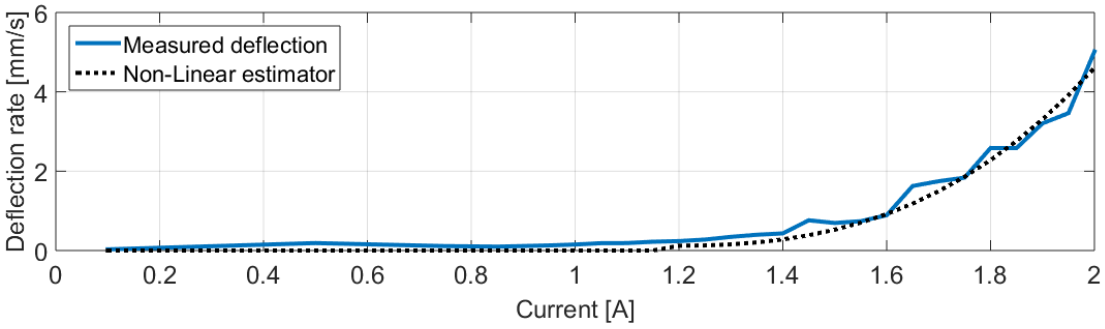

Figure 3-2: SMA-based actuator measured deflection rate per amplitude of the input current. This deflection rate was experimentally determined by applying a constant current for a duration of 1 second at 0.1 ampere intervals.

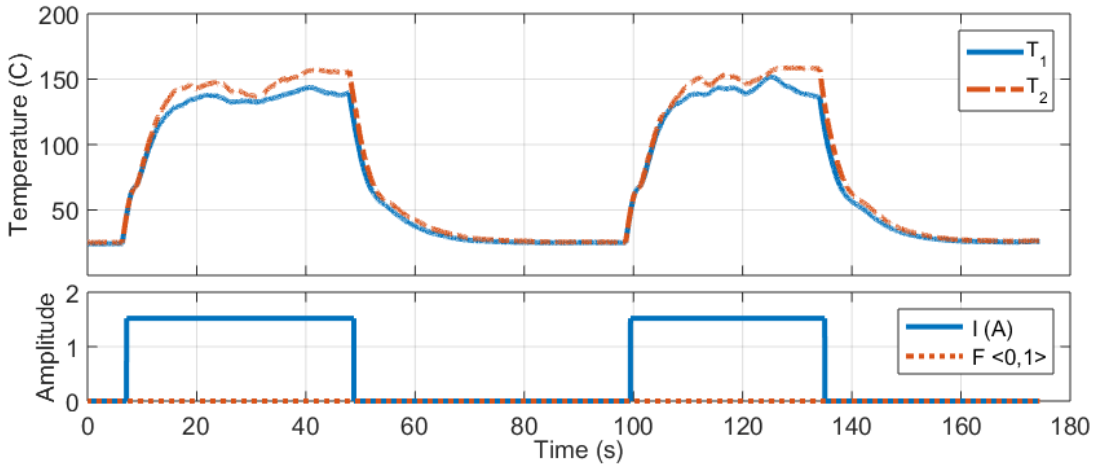

Figure 3-3: Temperature response of an SMA actuator when a constant current of 1.5 amperes is switched on and off at intervals. The temperature response was recorded with an infrared thermal imaging camera [25].

rate is not constant and that the deflection rate of the actuator is therefore not constant. This would mean that the response is non-linear and could even be quite erratic. An approach which linearizes the system as much as possible is required.

Multi Input, Single Output System Two cooling inputs have been added to the SMA-based actuator in order to maximize the bandwidth of the actuator. The presence of four inputs with only one output, rendering the system a MISO system, not only complicates control but also modeling of the actuator. A relative gain analysis can be performed for each subsystem to determine the influence of each input on the response of the total system. Finally, an approach will be required which translates the single available output of the system into the four inputs for the system. This approach may not destabilize the actuator and also not interfere with any of the compensation methods that are used

for the other challenges that have been discussed.

3-2 Requirements for the General Control Framework

The goal for the general control framework is to linearize the error $e(t)$ to the output $x(t)$ in a feedback configuration as depicted in Figure 3-4. The control framework will also need to solve the problems as described in the previous section. The objectives for the control framework can be defined as:

- Control both heating and cooling for two wires using only one measured output (MISO system)
- Compensate for hysteresis
- Compensate for non-linear response
- Maximize bandwidth

Additionally, two conditions are set to ensure a safe operation of the actuator and to enable the modular actuator to be extended easily. These conditions are:

- Constrain power output to prevent wire or nylon encasing from melting
- Limit computational complexity of control framework

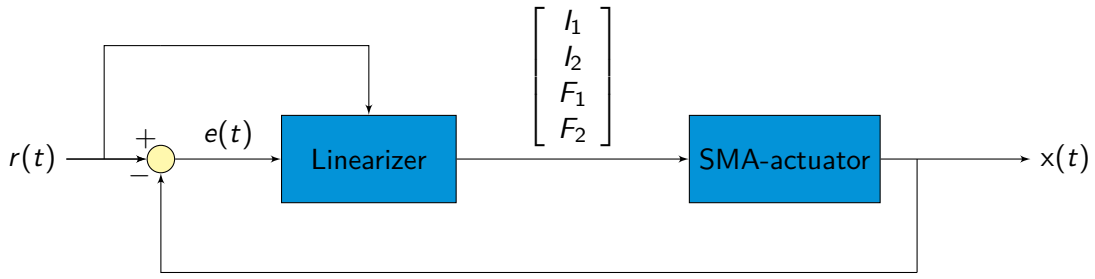

Figure 3-4: Linearized SMA-based actuator in feedback configuration

3-3 State-of-the-art Control

A review on state of the art controllers that have contributed to the development of this general control framework was performed during the literature survey [5]. The state-of-the-art include several types of control strategies such as:

- Pulse Width Modulation (PWM)
- Proportional, Integral and Derivative (PID) Control
- Iterative Learning Controller (ILC)
- Adaptive Control

- Fuzzy Logic Control
- Sliding Mode Control (SMC)

A lot of the control strategies employ models, or an approximation of the model in the form of a trained Neural Networks (NN) [26]. Due to the complexity of the modeling methods that have been discussed in Chapter 2, most of those control strategies have to be eliminated as candidates for a general control framework. The control strategies seem to use methods which are not based on the fundamental properties of the SMA. To establish a general control framework which is valid for all SMA-based actuators this is a strict requirement.

Furthermore, in the literature that has been reviewed only *one* control strategy was found that actively controlled the cooling [4] This control strategy uses a fuzzy logic controller to calculate a proportional gain for the four inputs of the system. It achieves a bandwidth of approximately 1 Hz which is higher than the other control strategies have achieved with a similar SMA.

It is unclear which control strategy is best suitable as a general control framework for a MISO SMA-based actuator since most of them are not usable for a multi-input systems or they use very actuator specific models or control strategies.

3-4 Phase Transformation Approach

A difficulty in controlling SMA-based actuators is that they consist of a number of complex subsystems, as depicted in Figure 3-5. The actuator can be split up into three subsystems:

G_1: Subsystem that converts the current and airflow into two temperatures
G_2: Subsystems that converts the two temperatures T_1 and T_2 into stress of the SMA wires
G_3: Subsystems that converts the stress of the SMA wires into the deflection of the actuator

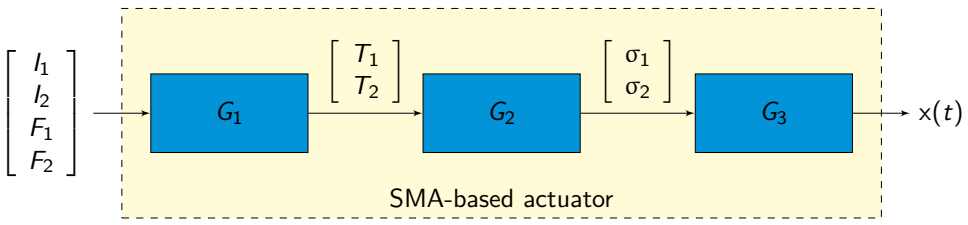

Figure 3-5: SMA-based actuator represented by three subsystems

For these three subsystems models are available. However, the question is: how accurate and reliable are these models? The temperature model for the first subsystem G_1 was

tested on 6 data sets, but it was unable to predict the erratic temperature fluctuations as depicted in 3-3. It was only sufficient for providing an estimation of the temperature of the SMA wires. The temperature of the SMA is very important for determining the development of stress in the SMA wires. This is because if the temperature is even 1 degrees Celsius below the austenite start temperature $A_s(\sigma)$, no phase transformation will occur. Since the first model was unable to provide an accurate estimate of the temperature of the SMA, all the models have been deemed insufficient for use in this control framework. Instead of using these models, the phase transformation approach is proposed.

The phase transformation approach focuses on triggering the desired phase transformation for a SMA actuator when it is required. This means that the focus is not on an exact temperature, but on a certain temperature *region*. These regions are defined as (3-1). If the control framework controls the inputs as such that the temperature of the SMA wires are safely within the required regions it can guarantee the corresponding transformations. The most important condition is that the temperature needs to either exceed $A_s(\sigma)$ or be lower than $M_s(\sigma)$ if, respectively, the stress of the SMA actuator needs to increase or decrease.

$$\begin{array}{llllll} \text{Region} & I: & & T & < M_s(\sigma) & \rightarrow \text{Forward transformation of SMA} \\ \text{Region} & II: & M_s(\sigma) < & T & < A_s(\sigma) & \rightarrow \text{No transformation of SMA} \\ \text{Region} & III: & A_s(\sigma) < & T & & \rightarrow \text{Reverse transformation of SMA} \end{array} \tag{3-1}$$

3-5 Control Principles

This section will elaborate on the different principles that are used to implement the phase transformation approach and how they compensate for the problems of SMA-based actuators as discussed in Section 3-1. Section 3-5-1 will investigate the relative gain of the four inputs. These four inputs will become a function of the error $e(t)$ and the reference $r(t)$ as depicted in Figure 3-4. When the four inputs have been paired, the next two control laws are introduced. These control laws will calculate the values for the appropriate inputs. They contain a threshold value to compensate for the hysteresis, a proportional gain and a derivative gain. Since these control laws are not active all the time, a Feed Forward (FF) control law is devised that ensures that the actuator stays stable at a certain position once it reaches it and the error becomes zero. The structure of the general control framework is depicted in Figure 3-6. The hierarchy of the control elements is defined within the input pairing block.

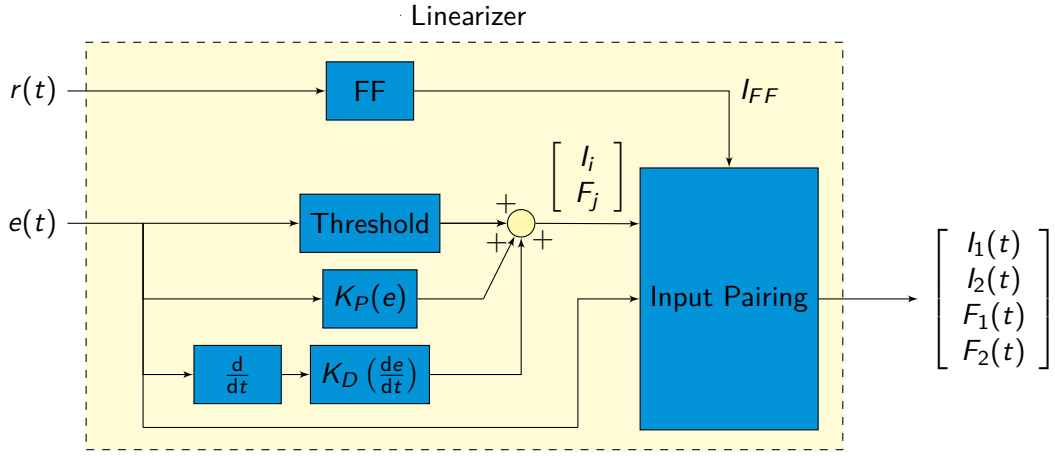

Figure 3-6: Schematic showing the inside of the linearizer of the proposed control framework. The blocks $K_P(e)$ and $K_D\left(\frac{\mathrm{de}}{\mathrm{d}t}\right)$ represent the functions for the current and the valve aperture as a function of respectively the error $e(t)$ or the derivative of the error $^{\mathrm{de}}/_{\mathrm{d}t}$.

3-5-1 Input Pairing

The linearizer block as depicted in Figure 3-4 will determine the required inputs for the system based on the error $e(t)$. This requires the pairing of the inputs which can be achieved by considering the gain matrix of the whole system. The gain matrix consists of entries which indicate the influence of an input to a certain output. An example is given in Table 3-1. The entries in the gain matrix will not be represented by numbers but by either a positive sign, a zero or a negative sign since the analysis is done for the general configuration and that the exact value is not yet important at this point. For the analysis, the subsystems will be analyzed in the reverse order. The gain matrix analysis for subsystem G_3 and G_2 are valid for certain conditions which describe the mechanics of the nylon polymer beam and the phase transformations of the SMA.

Table 3-1: Example of a gain matrix for a system with two inputs and two outputs

		Inputs	
		u_1	u_2
Outputs	y_1	$K_{11} = \frac{\Delta y_1}{\Delta u_1}\Big\vert_{u_2}$	$K_{12} = \frac{\Delta y_1}{\Delta u_2}\Big\vert_{u_1}$
	y_2	$K_{21} = \frac{\Delta y_2}{\Delta u_1}\Big\vert_{u_2}$	$K_{22} = \frac{\Delta y_2}{\Delta u_2}\Big\vert_{u_1}$

Subsystem G_3 Subsystem (3-2) has the inputs σ_1 and σ_2 and has one output x(t). The inputs are either greater than or equal to zero since the SMA wires can only subjected to a tension. The gain matrix analysis yields the results in (3-3), which are derived from the conditions of the movement of the actuator as defined in (3-4). It is clear that the two inputs have the opposite effects on the output.

$$\mathrm{x}(t) = G_3 \begin{bmatrix} \sigma_1 \\ \sigma_2 \end{bmatrix} \tag{3-2}$$

$$K_{G_3} = \begin{bmatrix} + & - \end{bmatrix} \tag{3-3}$$

$$\frac{d\mathrm{x}(t)}{dt} \begin{cases} > 0, & \{\sigma_1 \mid \sigma_1 > 0 \text{ and } \sigma_1 > \sigma_2\} \\ = 0, & \{\sigma_1, \sigma_2 \mid \sigma_1 = \sigma_2\} \\ < 0, & \{\sigma_2 \mid \sigma_2 > 0 \text{ and } \sigma_2 > \sigma_1\} \end{cases} \tag{3-4}$$

Subsystem G_2 The subsystem (3-5) represents the phase transformation of the SMA and the stress in the SMA actuators. It has two inputs, T_1 and T_2 and has two outputs, σ_1 and σ_2. The gain matrix of subsystem G_2 with conditions as defined in (3-7) is defined as (3-6). This gain matrix is only valid under the assumption that the SMA enclosure provides sufficient insulation to prevent T_1 from influencing T_2 and vice versa.

$$\begin{bmatrix} \sigma_1 \\ \sigma_2 \end{bmatrix} = G_2 \begin{bmatrix} T_1 \\ T_2 \end{bmatrix} \tag{3-5}$$

$$K_{G_2} = \begin{bmatrix} + & 0 \\ 0 & + \end{bmatrix} \tag{3-6}$$

$$\frac{d\sigma_i(t)}{dt} \begin{cases} > 0, & \{T_i \mid T_i > A_s(\sigma_i)\} \\ = 0, & \{T_i \mid M_s(\sigma_i) < T_i < A_s(\sigma)\} \\ < 0, & \{T_i \mid T_i < M_s(\sigma)\} \end{cases} \tag{3-7}$$

Subsystem G_1 The subsystem (3-8) has four inputs, $\begin{pmatrix} I_1 & I_2 & F_1 & F_2 \end{pmatrix}$ and two outputs $\begin{pmatrix} T_1 & T_2 \end{pmatrix}$. The conditions for this system are stated in (3-10). They basically state that the temperature T_i will change as long as the equilibrium temperature $T_{i,\mathrm{eq}}$ has not been reached, or that the temperature will increase or decrease when, respectively, I_i or F_i are increased.

$$\begin{bmatrix} T_1 \\ T_2 \end{bmatrix} = G_1 \begin{bmatrix} I_1 \\ I_2 \\ F_1 \\ F_2 \end{bmatrix} \tag{3-8}$$

$$K_{G_1} = \begin{bmatrix} + & 0 & - & 0 \\ 0 & + & 0 & - \end{bmatrix} \tag{3-9}$$

$$\frac{dT_i(t)}{dt} \begin{cases} > 0, & \{I_i, F_i \mid T_i < T_{i,\mathrm{eq}}(I_i, F_i) \text{ or } \frac{dI_i}{dt} > 0\} \\ = 0, & \{I_i, F_i \mid T_i = T_{i,\mathrm{eq}}(I_i, F_i) \text{ and } \frac{dI_i}{dt}, \frac{dF_i}{dt} = 0\} \\ < 0, & \{I_i, F_i \mid T_i > T_{i,\mathrm{eq}}(I_i, F_i) \text{ or } \frac{dF_i}{dt} > 0\} \end{cases} \tag{3-10}$$

Linearizer subsystem The linearizer subsystem, as introduced in Figure 3-4, will transform the error $e(t)$ into the correct inputs for the SMA-based actuator. This requires a pairing of the four inputs and representing them as a function of $e(t)$. Since the subsystems are subject to some discontinuous conditions, the resulting pairing function will also be discontinuous. The gain matrix for the complete system as defined by (3-11) is evaluated, resulting in the gain matrix (3-12). The gain matrix clearly indicates that there are input pairs; the pair I_1 and F_2 which have a positive gain and the pair I_2 and F_1 which have a negative gain.

$$\mathrm{x}(t) = G_3 G_2 G_1 \begin{bmatrix} I_1 \\ I_2 \\ F_1 \\ F_2 \end{bmatrix} \tag{3-11}$$

$$K_{G_1,G_2,G_3} = K_{G_3}\, K_{G_2}\, K_{G_1} = \begin{bmatrix} + & - & - & + \end{bmatrix} \tag{3-12}$$

Switching between the two input pairs can be achieved by looking at the sign of the error $e(t)$. If the error is positive the inputs I_1 and F_2 should be used and if the error is negative then the inputs I_2 and F_1 should be used. The values that have to be used either for I_i or F_j is determined in the subsections.

To prevent the control framework from switching at a very fast rate between the two inputs, a boundary e_{boundary} is defined. This will ensure that the controller only switches from the input pair when the absolute value of the error exceeds the error boundary value and if the sign of the error changes.

3-5-2 Response Threshold

The next problem of the SMA-based actuator that is addressed is the response threshold. The problem with most of the control strategies used for SMA-based actuator is that they do not consider the fact that for the SMA-actuator to respond either condition (3-13) or condition (3-14) must be met, depending on which transformation of the SMA is required. If these conditions are met, the controller can ensure that the SMA actuator responds.

$$T_i > A_s(\sigma_0), \quad (\textit{Reverse transformation}) \tag{3-13}$$

$$T_i < M_s(\sigma_0), \quad (\textit{Forward transformation}) \tag{3-14}$$

The condition can be extended to calculate the corresponding values for the current (3-15) and the valve aperture (3-16). The equation for the threshold value for the current, $I_{\text{threshold}}$, is obtained by rewriting (2-18). It is a function of the desired temperature

and an airflow of $F = 0$ and the reference temperature needs to comply to $T_{i,\text{ref}} \geq A_s(\sigma_0)$. Determining the threshold for the valve aperture is a more difficult case since temperature is unknown. The threshold value for the valves needs to be chosen such that they result in a quick drop of the temperature of the SMA to a temperature below the martensitic starting temperature. Since the phase transformation state of the actuator, i.e. in what temperature region it is, is unknown there is no definitive value to be determined. The only knowledge available is that the temperature of the SMA actuator is within one of the three temperature regions. However, since the requirement states that the temperature must be lower than $M_s(\sigma_i)$, any arbitrary value for $F_{\text{threshold}}$ can be set. Any value larger than zero ensures that the SMA actuator starts to cool down and that the stress is minimized. This value can also be coupled to a minimal value for the airflow to start to flow through the valve, but this depends on the hardware that is used. The threshold values are the *minimum* value for the current and valve aperture when control is active, i.e. $|e(t)| \geq e_{\text{boundary}}$.

$$I_i \geq I_{\text{threshold}} = \sqrt{\frac{mc_p\left(T_{i,\text{ref}} - T_\infty\right) + A_{\text{SMA}}h(F)\left(T_{i,\text{ref}} - T_\infty\right)}{R\left(T_{i,\text{ref}}\right)}} \tag{3-15}$$

$$F_j \geq F_{\text{threshold}} \geq F_{\text{valve,min}} \tag{3-16}$$

3-5-3 Linearization of SMA response

Now that the hysteresis effect has been compensated for, the next step is to linearize the inputs to the change in temperature. The control inputs influence the change in temperature in the terms $\dot{Q}_{\text{in}}$ (2-15) and $\dot{Q}_{\text{out}}$ (2-16). The term $\dot{Q}_{\text{in}}$ is quadratic in I_i. To linearize this term, the square root of the absolute value of the error must be used for the calculation of the proportional gain $K_{P,I}$ as in (3-17). This should result in an equilibrium temperature that is proportional to the current I_i (3-18).

$$I_{i,KP} = K_{P,I}\sqrt{|e(t)|} \tag{3-17}$$

$$T_{i,\text{eq}} \propto I_i \tag{3-18}$$

The term $\dot{Q}_{\text{out}}$ is slightly non-linear in F_i since the heat transfer coefficient $h(F_i)$ is non-linear in F_i as can be seen in Figure 3-7. However, in the range of the control variable F_i the non-linearity is not apparent, hence a linear approximation is used. Any proportional gain for valve aperture is therefore calculated by just using the absolute value of the error (3-19).

$$F_{j,KP} = K_{P,F}\,|e(t)| \tag{3-19}$$

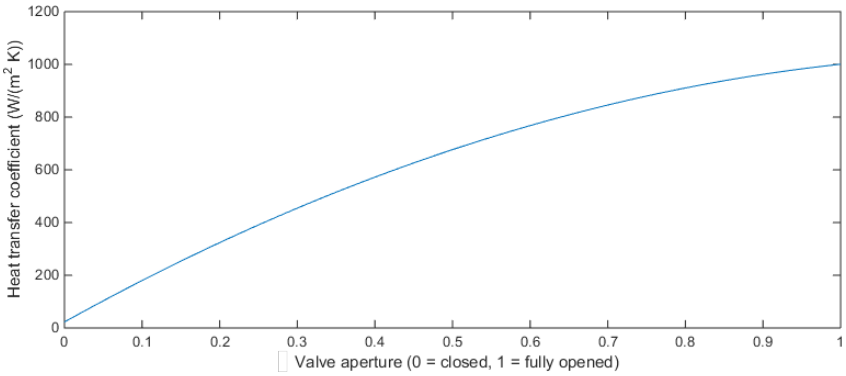

Figure 3-7: Heat transfer coefficient as a function of the valve aperture F_i over its full input range of <0,1>, obtained from experimental data [4].

This linearization is valid under the assumption that the phase transformation process is linear in the power input and output to the SMA actuators, i.e. the terms $\dot{Q}_{\text{in}}$ and $\dot{Q}_{\text{out}}$. Experiments have to determine whether that assumption is correct.

3-5-4 Bandwidth Optimization

The bandwidth of an SMA actuator is generally low, somewhere in the order of 0.1 to 0.3 Hz. If these actuators are to be used in applications such as wind turbines, the bandwidth needs to be increased. Increasing the bandwidth of the SMA-based actuator is achieved with two complementary control strategies.

1. **Pole/zero cancellation**
   The Bode plot in 3-1 of the SMA actuator indicates the presence of at least one slow pole at approximately 0.8 rad/s. By feeding the error signal through a filter that has a zero at that frequency, the slow pole is canceled. Since applying a single zero would mean that the gain in that filter would be unlimited for high frequencies, another pole needs to be added. Since noise is usually present at higher frequencies in real systems (noise from sensors etc.), an additional pole is added at a higher frequency. This extra pole will reduce the gain for high frequencies and thus filter out the effects of the noise on the system. The resulting filter is defined as (3-20) with an example Bode plot as depicted in Figure 3-8.

$$H_1(s) = \frac{{}^1\!/_{z_1}s + 1}{({}^1\!/_{p_1}s + 1)({}^1\!/_{p_2}s + 1)} \tag{3-20}$$

   The effects of the filter can be demonstrated by applying them to the temperature model of the SMA actuator. The filter increases the initial input which results

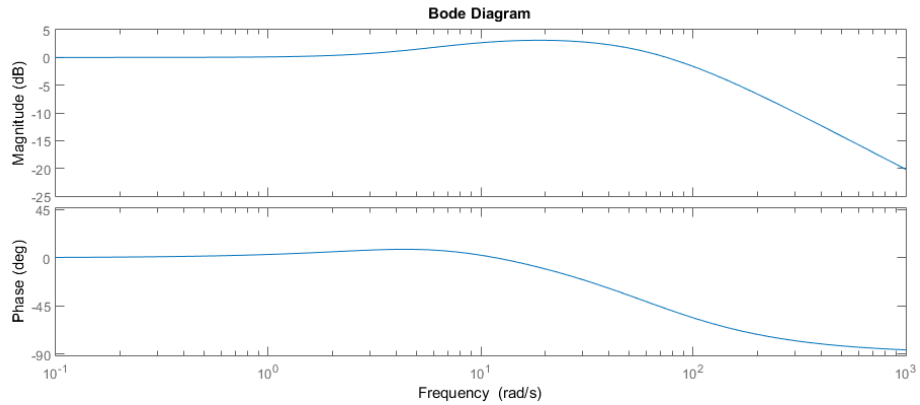

Figure 3-8: Filter used to increase bandwidth and filter out high frequency noise

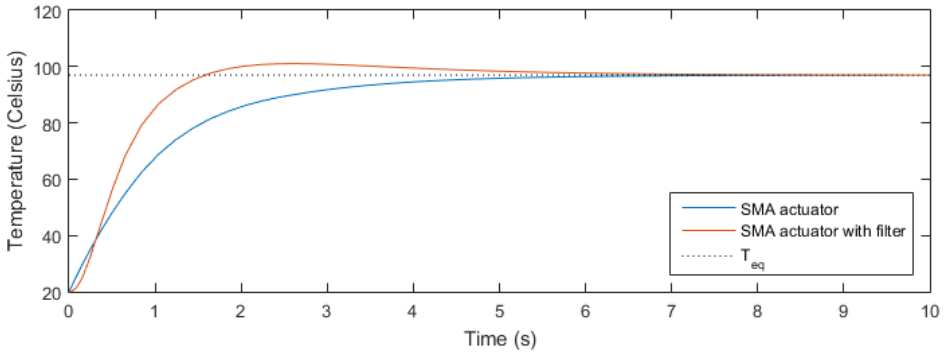

Figure 3-9: Simulation of the effects of the filter on the evolution of the temperature of a SMA actuator

in a faster increasing temperature, as can be seen in Figure 3-9. The equilibrium temperature is reached faster and since the phase transformation rate and therefore also the actuator response rate is relative to this temperature, the bandwidth of the actuator increases.

2. **Derivative control**
   To further increase the bandwidth and also the performance of the actuator in terms of reference tracking capabilities, a derivative control element is added to the linearizer control law as depicted in 3-4. This derivative control element increases or decreases the gain according to the magnitude and sign of the derivative. The resulting derivative control laws are defined as (3-21) and (3-22).

$$I_{i,KD} = \text{sign}\left(\frac{\mathrm{d}e}{\mathrm{d}t}(t)\right) K_{D,I} \left|\frac{\mathrm{d}e}{\mathrm{d}t}(t)\right| \tag{3-21}$$

$$F_{j,KD} = \text{sign}\left(\frac{\mathrm{d}e}{\mathrm{d}t}(t)\right) K_{D,F} \left|\frac{\mathrm{d}e}{\mathrm{d}t}(t)\right| \tag{3-22}$$

3-5-5 Feed Forward Stabilizer

Depending on the application of the SMA-based actuator, it may be desirable to attain a certain position x with the actuator, where $\mathrm{x} \neq \mathrm{x}_0$. Keeping the actuator at fixed deflection means that after the actuator reaches that position, the stresses σ_1 and σ_2 must be kept constant. It also means that the strain in the SMA actuators is constant, and thus that the derivative of the strain $\dot{\varepsilon}(t)$ is equal to zero. This permits the use (2-13) to compose a FF stabilizer strategy. First, the term $\Delta\mathrm{x}$ is defined as the offset of $\mathrm{x}(t)$ to the neutral axis of the SMA-based actuator (3-23).

$$\Delta\mathrm{x} = \mathrm{x}(t) - \mathrm{x}_0 \tag{3-23}$$

The stabilizer feed forward current is determined as (3-24), where I_{FF} is a constant and $K_{\mathrm{FF},I}$ is a proportional gain on the absolute value of the offset of $\mathrm{x}(t)$ to the neutral axis of the SMA-based actuator. The term I_{FF} is related to the hysteresis problem. It ensures a certain temperature where the stress will be greater than σ_0. The second term, $K_{\mathrm{FF},I}$ will be proportional to the term c in (2-13). This proportionally increases the stress σ_i as $\Delta\mathrm{x}$ increases.

$$I_{\text{stabilizer}} = I_{\mathrm{FF}} + K_{\mathrm{FF},I} \left|\Delta\mathrm{x}\right| \tag{3-24}$$

The FF stabilizer is only active when the absolute value of the error is within the error boundary, i.e. $|e(t)| \leq e_{\text{boundary}}$. The sign of $\Delta\mathrm{x}$ determines which of the two inputs, I_1 or I_2, is used. The current $I_{\text{stabilizer}}$ is smaller than the current that will be used for control when the error exceeds the error boundary.

Control of the airflow will only be used by the FF stabilizer when the reference equals the neutral position x. Then both valves are opened allowing for cooling of both SMA actuators. This will results in the stresses σ_1 and σ_2 returning to σ_0. When the reference is not equal to x_0, the control of the airflow will be performed by the other control strategies as discussed in this subsection. By switching from the normal control laws to only the FF control law, the energy input to the system already decreases. Since the energy input decreases, the temperature should decrease. This already ensures that no further phase transformation occurs and that the stress in the SMA actuator remains constant.

3-6 Summary

The governing control law is obtained by combining the separate control elements as described in the Section 3-5, rendering them to (3-25) and (3-26). The minimum values are defined as (3-27) and (3-28). The threshold value and proportional gain are switched by the condition $|e(t)| \geq I_{\text{threshold}}$, but the derivative gain is not switched by that condition. This means that the derivative gain is active when the error is within the error boundary. This results in a damping effect of the actuation when the actuator has reached its reference position where $e(t) = 0$. The stabilizer current and airflow will also be active when the error is within the error boundary, where the current and the airflow are a function of Δx.

$$I_i = I_{\text{threshold}} + I_{i,KP} + I_{i,KD} \tag{3-25}$$

$$F_j = F_{\text{threshold}} + F_{i,KP} + F_{i,KD} \tag{3-26}$$

$$\min(I_i) = \begin{cases} I_{\text{stabilizer}}, & \text{if: } |e(t)| < e_{\text{boundary}} \\ I_{\text{threshold}}, & \text{if: } |e(t)| \geq e_{\text{boundary}} \end{cases} \tag{3-27}$$

$$\min(F_j) = \begin{cases} F_{\text{stabilizer}}, & \text{if: } |e(t)| < e_{\text{boundary}} \\ F_{\text{threshold}}, & \text{if: } |e(t)| \geq e_{\text{boundary}} \end{cases} \tag{3-28}$$

All of these control laws generate the control inputs as depicted in Figure 3-10. The gains that are used for these surfaces are not definitive values, they can be adjusted to decrease or increase aggressiveness of the controller. The steepness of the surface in the direction of the error can be increased by increasing $K_{P,I}$ or $K_{P,F}$. In the same way, the steepness of the surface in the direction of the derivative of the error can be increased by increasing $K_{D,I}$ or $K_{D,F}$. To increase the overall level of the entire surface, the threshold value can be increased. This might be necessary when the tension in the SMA actuators rise.

When the union of the control surfaces in Figure 3-11 is considered, a point with a minimum controller output can clearly be observed. This is the center point where both the error and its derivative are smaller than the error boundary value. The union of the control surfaces seems to mimic a surface that describes the energy for a system with a global energy minimum.

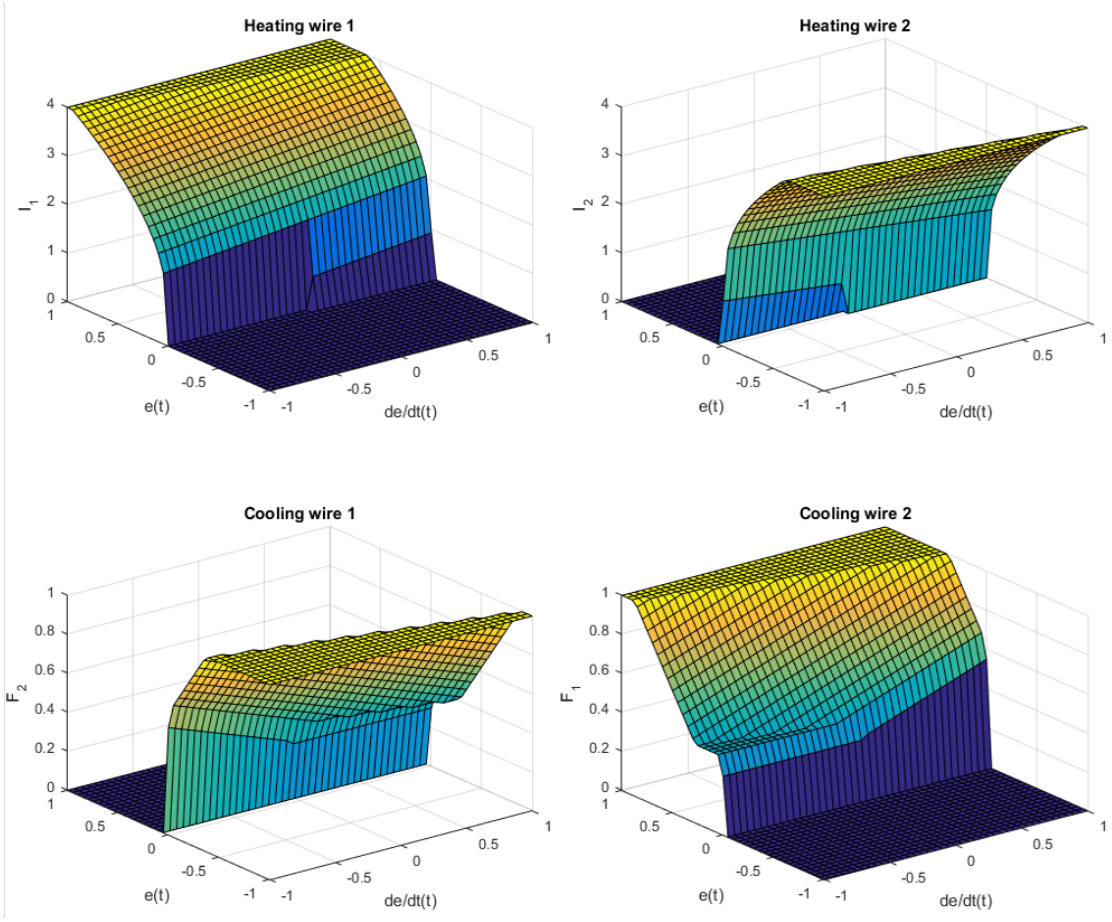

Figure 3-10: Control framework output values for the four inputs as function of the error and its derivative

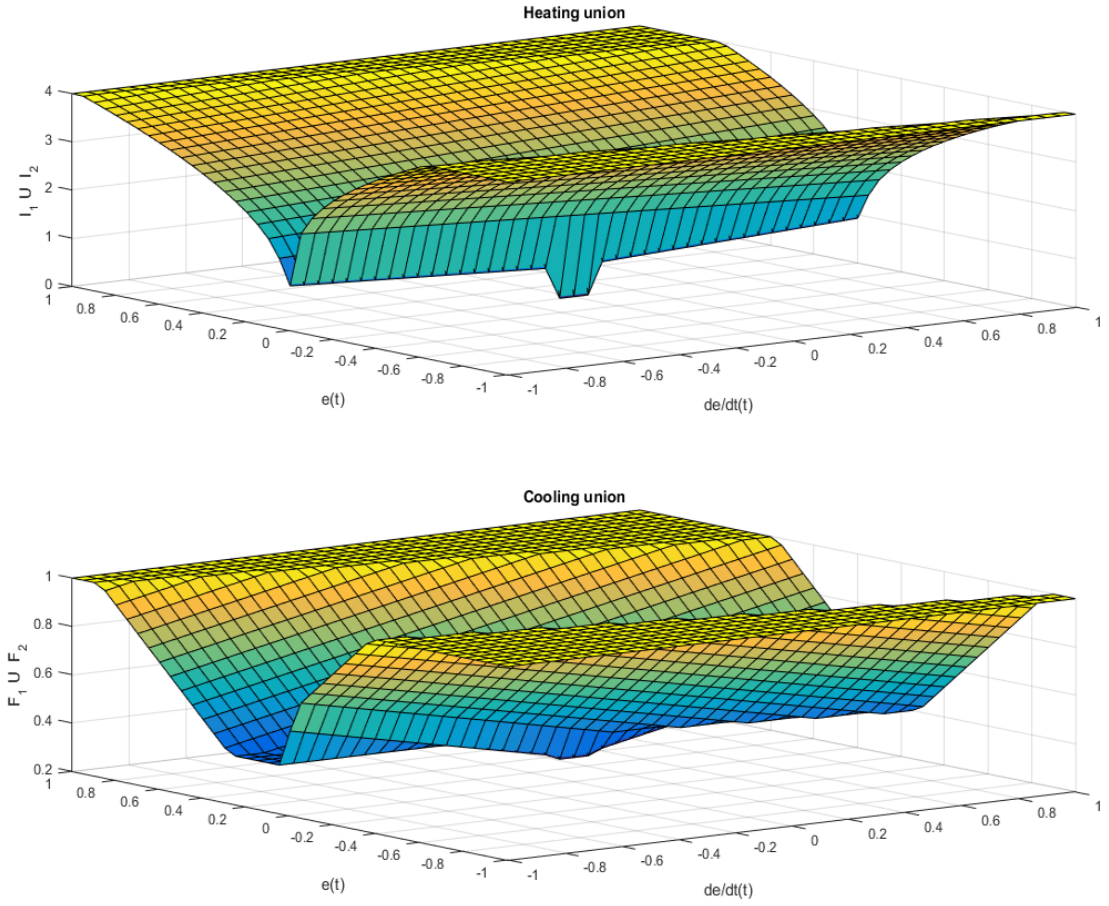

Figure 3-11: Union of the control inputs for heating and cooling as function of the error and its derivative

Part II

Practice

Chapter 4

Controller Implementation

This chapter will investigate the validity of the theories and the performance of the proposed general control framework as discussed in Chapter 3. It starts with an introduction to the Shape Memory Alloy (SMA)-based actuator and the rest of the hardware that was used for the experiments. The first experiments investigate the effectiveness and reliability of the individual control strategies for the challenges for control of SMA-based actuators, which were:

- Hysteresis
- Non-linear response
- Multi Input, Single Output (MISO) system
- Low bandwidth

4-1 Hardware

The SMA-based actuator that was used is depicted in Figure 4-1. It has a common ground connection terminal for the two SMA actuators and two separate positive connection terminals. Hollow bolts were used to connect the air hoses from the proportional valves. The valves have their own Pulse Width Modulation (PWM) signal generator and power supply. The current for the Joule heating of the SMA actuator was supplied by two controllable power supplies. The current that was supplied was controlled via an analog signal. Both the power supplies and the PWM signal generators were controlled using an Arduino board.

The schematic in Figure 4-2 illustrates how the hardware was configured. This section shortly elaborates on the hardware that was used for the experiments. More details of the hardware can be found in Appendix A.

Figure 4-1: Picture of the actuator with the connections indicated. The base indicates where the actuator is clamped into the setup and the tip of the actuator is where the deflection is measured.

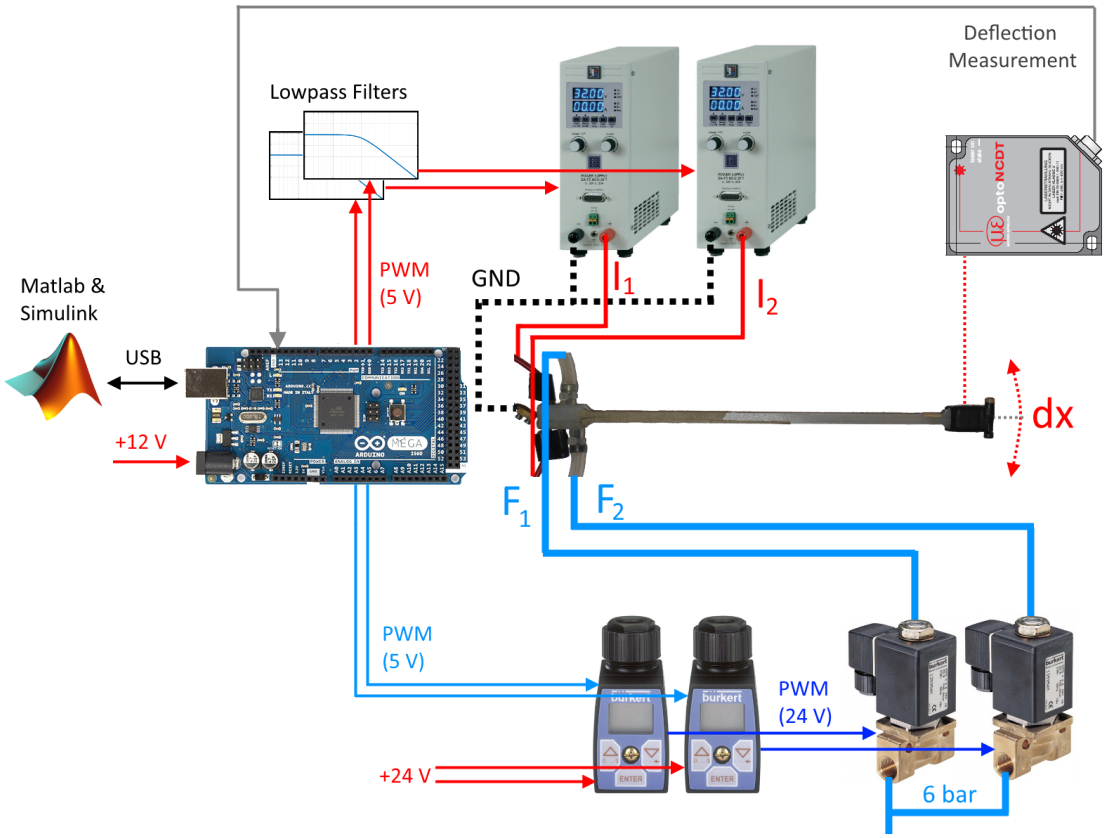

Figure 4-2: Illustration depicting the total hardware setup and connections.

I/O Interface

An Arduino Mega 2560 board had been selected to facilitate the input output interface and to run the controller algorithm. Motivation for the use of this board is that it is cheap, readily available and offers a good possibility for easy scaling for use with multiple modules. It was interesting to investigate the functionality and reliability of these reasonably new and upcoming low-cost systems.

All experiments were performed with a sampling rate of 50 Hz, allowing for identification of dynamics of the system up to a frequency of 25 Hz according to Shannon's sampling theorem [27]. The Arduino was connected to a computer running Matlab and Simulink. The computer itself was running Windows, which has a default USB sampling rate of 125 Hz, which is sufficient for the required sampling rate for the experiments of 50 Hz.

Arduino boards do not have an actual analog output, but they simulate analog outputs by using Pulse Width Modulation (PWM). Since the goal was to keep the currents as stable as possible, pin 4 and 13 are used for controlling the power supplies given that these pins run at a higher PWM frequency of 980 Hz instead of the standard 490 Hz. A higher PWM frequency will result in a smoother analog signal. The PWM signals are then fed through an analog low pass filter before they reach the power supplies.

The Arduino was programmed using Matlab and Simulink, which compiles the code to C or C++ and uploads it to the Arduino. The Arduino then runs the algorithm and sends data in real-time to Matlab for analysis. Initiating the compilation of the code to run externally on the Arduino could only be done manually, which drastically increased the time required to perform the experiments. An average experiment of 30 seconds required almost 90 seconds from compilation to the saving of the data.

Power Supply

The power supplies that were used are from Elektro Automatik (Type EA PS-8032-20T). These power supplies were configured as current sources, with a range from zero to a maximum of 20 Amperes. The current was controlled by applying a voltage on the analog input on the power supply.

Airflow Control

Control of the airflow through the channels in the SMA-based actuator was provided by valve controllers (Type 8605) and proportional valves (Type 2821) from Burkert. The PWM signal generators are required since the valves operate at 24 Volts and the Arduino board can only supply a 5 Volts PWM signal. The valve controllers from Burkert serve as an amplifier of the PWM signal from the Arduino.

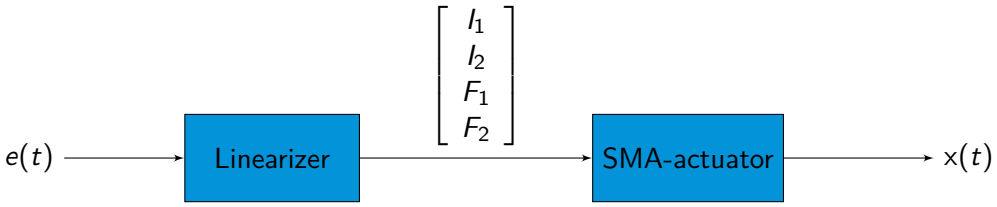

Figure 4-3: Linearized SMA-based actuator in feedback configuration

Displacement Sensor

The sensor that was used to measure the deflection of the SMA-based actuator was the Micro Epsilon optoNCDT 1401. It is a laser position sensor with a range of 20 millimeters and is configured such that the center position of the measurement range corresponds to the neutral position x_0 of the actuator. The maximum observable displacement in both negative and positive x direction was 10 millimeter.

4-2 Control Principles

In Section 3-1 some of the difficulties with control of SMA actuators were discussed. In this section, the effectiveness of the individual control laws as proposed in Section 3-5 are investigated before testing the Phase Transformation Approach as a whole.

4-2-1 Hysteresis

The hysteresis for the actuator has already been shown in Figure 3-2. It shows that the actuator does not (or barely) respond for currents lower than approximately 1.2 Amperes. For currents that exceed this value the actuator does deflect.

An experiment was carried out where different step inputs were directly put on the input of the linearizer ($e(t)$). The controller parameters that were used for this experiment are listed in Table 4-1. The results are shown in Figure 4-4. It can be observed that the actuator responds for any input that is larger than zero. This means that the hysteresis of the SMA actuators is no longer a problem.

Table 4-1: Controller parameters used for testing solutions for the hysteretic and non-linear response.

	Threshold	K_P	K_D
I_i	1.25	8	1
F_i	0.5	0.5	0

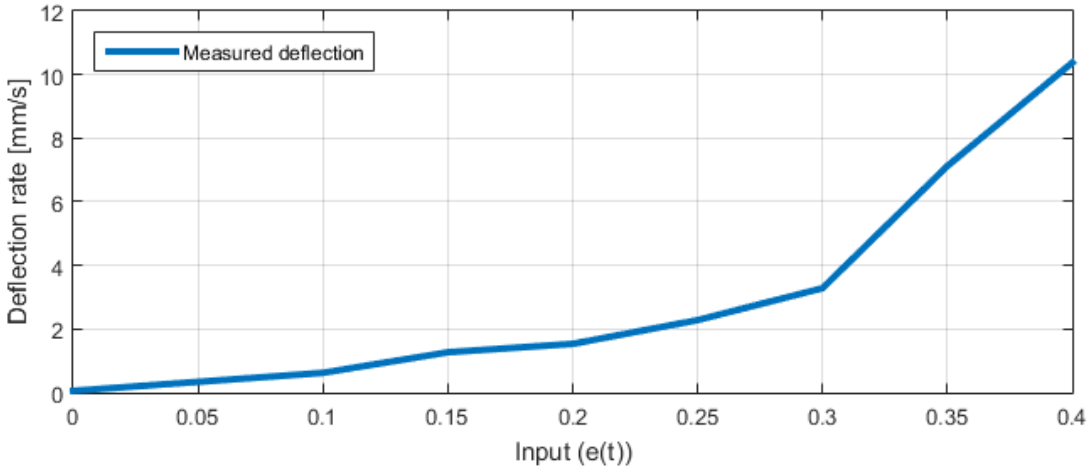

Figure 4-4: Deflection rate of the SMA-based actuator to different step inputs on the input of the linearizer. The error $e(t)$ correspond to the voltage difference that is measured by the laser, where 0.1 Volts equals 0.5 millimeters. The input range on this graph therefore corresponds to an error of 0 to 2 millimeters.

The controller with the threshold value is compared to a similarly structured controller without the threshold value, which is a simple Proportional and Derivative (PD) controller. The performance of the simple PD controller is shown in Figure 4-5. It is clear from this figure that there is a delay in the response for the PD controller. The PD controller with the threshold values has a better response, though it is very sensitive to the proportional control parameter. If the proportional gain is too high, overshoot occurs when the reference signal changes direction (small peak at 8.2 seconds).

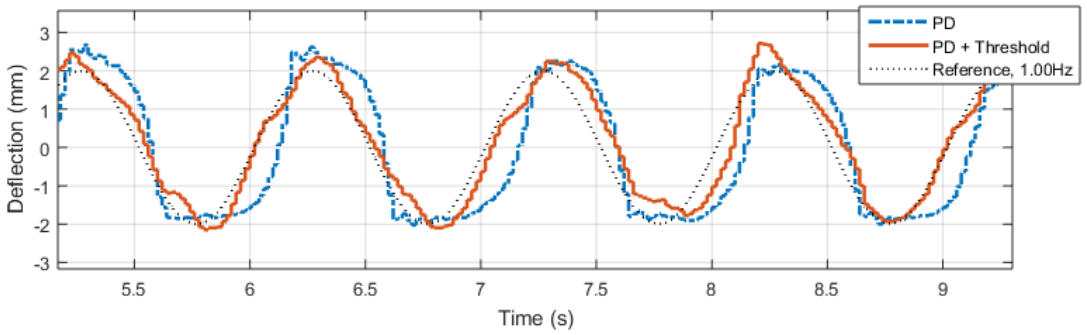

Figure 4-5: Tracking of sinusoidal signal at 1 Hz for PD controller with and without threshold value for SMA-based actuator. Both controllers use the same structure except for the threshold value.

For some threshold values the controller shows good performance, but when the frequency or amplitude is increased or if the threshold value is slightly increased, the performance drastically decreases. This effect can be observed in 4-6, where the thresh-

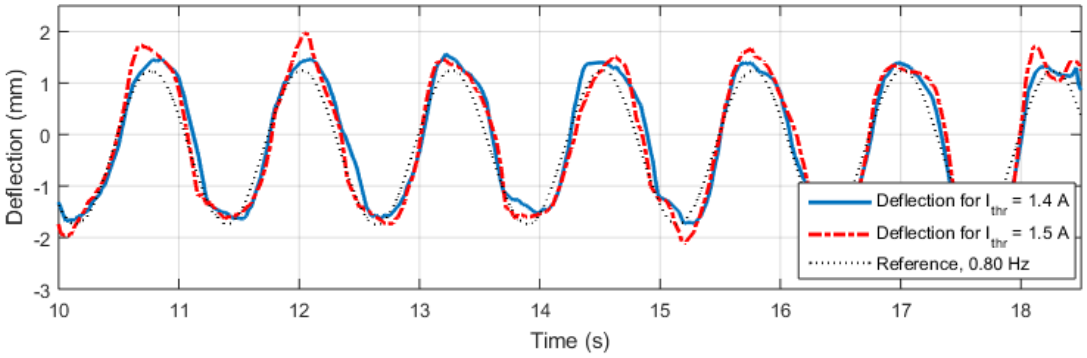

Figure 4-6: Graph depicting effect of increase the threshold value for the current I_i by 0.1 amperes. By increasing the threshold value (dash-dotted line), the controller becomes too aggressive causing the actuator to overshoot at the point where the reference signal peaks.

old value for the current is slightly increased by 0.1 amperes. This causes the actuator to overshoot at the point where the reference signal peaks. If the threshold value is further increased or if the frequency or amplitude of the reference signal is increased, the overshoot also increases.

4-2-2 Linearization

From Figure 3-2 it can be observed that once the input exceeds the threshold value that the increase of the actuator deflection rate is not linearly proportional to the increase in the current. To see if the response of the actuator is now linear in the input, Figure 4-4 needs to be examined. For the first part, for an input up till 0.3 it can be observed that the response is linear. Though from inputs greater than 0.3 the actuator response increases non-linear. The proposed control law for the linearization does not achieve a linear response over the possible input range, which is even larger than the depicted input range in Figure 4-4. The linear regime can defined as inputs from zero up until 0.3. Beyond this point the response seems to be linear again, but not with the same gradient. Inputs larger than 0.4 were not tested since they saturated the output within less than half a second.

4-2-3 Bandwidth Optimization

The optimization of the bandwidth was achieved by means of two control principles; a bandwidth filter and a gain on the derivative of the error. The effects of the bandwidth filter are first discussed, which affects the whole Single Input, Single Output (SISO) system of $e(t)$ to $\mathrm{x}(t)$. The derivative gain applies to the subsystems, of which the effects are hard to identify.

Bandwidth Increasing Filter

To identify the frequency response of the SMA-based actuator with the proposed control framework, an experiment was designed using the control structure as in 4-3. The system is tested with and without the filter that was designed to increase the bandwidth of the actuator. For the data collection for the identification of the dynamics of the set-up, a Random Binary Signal (RBS) is chosen as an the input signal $u(t)$ (4-1), where $w(t)$ is stochastic white noise and d is the amplitude of the RBS.

$$u(t) = d \cdot \text{sign}\left[w(t)\right] \tag{4-1}$$

This signal was selected since it has the following advantages for this system:

- $u(t)$ covers the wide frequency spectrum of a white noise. For a frequency response identification it is desired that the obtained output data contains information on the system over a sufficiently wide frequency range. In order to obtain data that complies to that requirement, the input signals have to be sufficiently exciting, and thus have a spectrum that covers a wide frequency range.
- $u(t)$ is bounded in amplitude. This is favourable since it can therefore be set to only excite the linear dynamics. In 4-2-2 a linear regime of the system was found.
- $u(t)$ is binary. This is desirable since the power will therefore be maximal under an amplitude bound, and thus the signal-to-noise ratio will be high at the output.

The actual frequency response was obtained by means of an Empirical Transfer Function Estimate (ETFE), defined as the expression (4-2). It represents the frequency response and is equal to the quotient of the Fourier transforms of the input signal $u(t)$ and the output signal $y(t)$.

$$\breve{G}_N(e^{i\omega}) := \frac{Y_N(\omega)}{U_N(\omega)} \tag{4-2}$$

- **Without filter**
  The ETFE yields the frequency response as depicted in 4-7a. The dots represent the raw data obtained from the experiment and the solid line represents the re-sampled and smoothed data. The frequency response shows a gain margin of 3.67 dB (19.89 Hz) and a phase margin of 96.7 degrees (2.46 Hz). This means that at a frequency of 2.46 Hz, the response suffers from a delay of approximately 0.11 seconds. This suggests that the actuator is stable and that the bandwidth has been increased to 2.46 Hz. However, this is only valid for inputs that are within the linear regime as defined in Section 4-2-2.

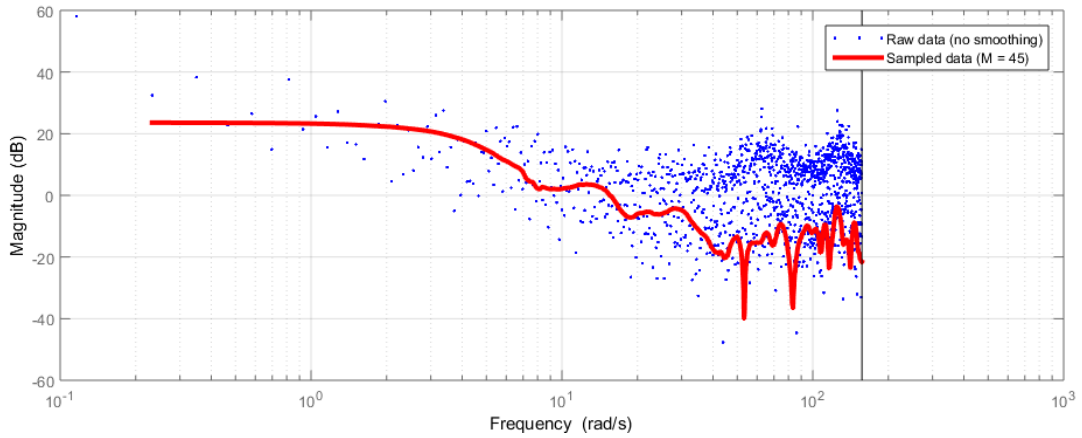

(a) Without bandwidth filter

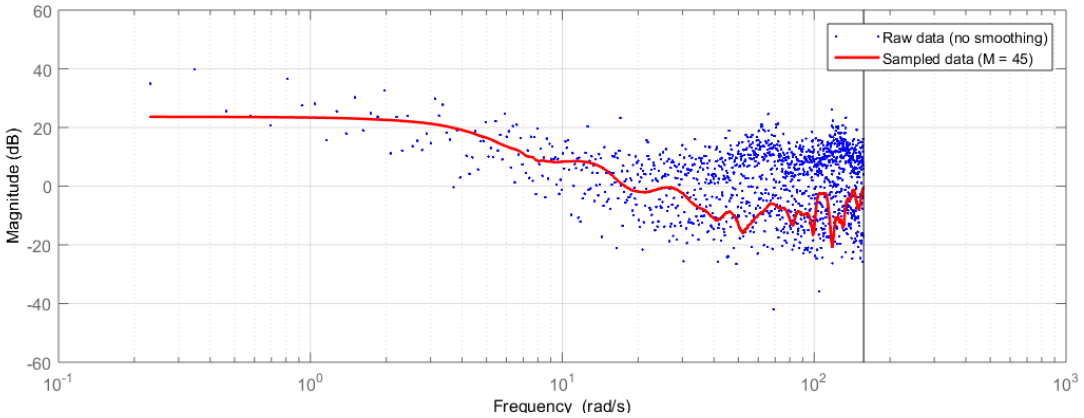

(b) With bandwidth filter

Figure 4-7: ETFE obtained frequency response of SMA-based actuator with proposed control framework without the bandwidth filter. The dots represent the ETFE for the raw and unsampled data and the solid line represents ETFE for the resampled and smoothed data.

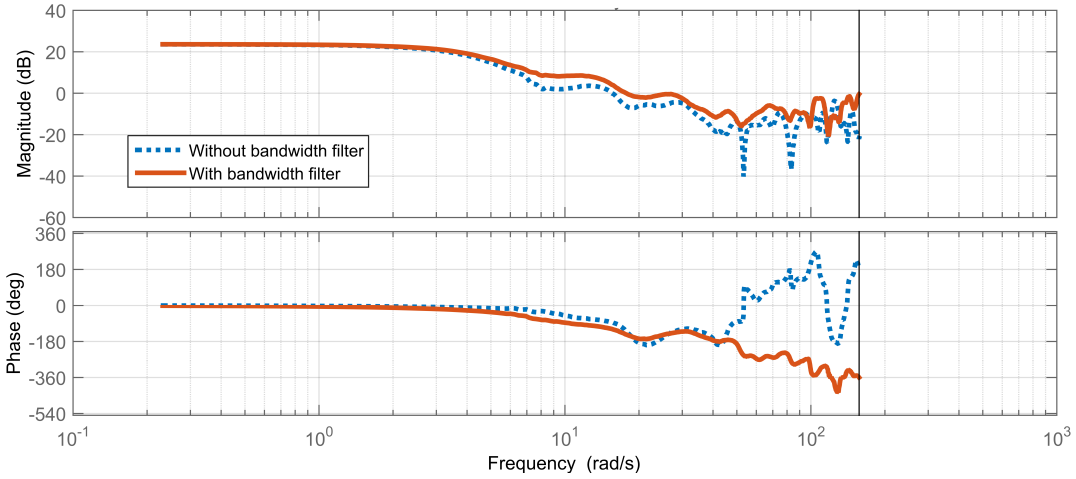

Figure 4-8: ETFE frequency response obtained from experiments.

- **With filter**
  The ETFE for the system with bandwidth filter is depicted in 4-7b. A comparison between the two identified systems is shown in the bode plot in Figure 4-8. It shows that the bandwidth is increased, from approximately 2.46 Hz to 2.83 Hz.

Derivative Gain

The effects of the derivative gain are hard to represent in a frequency response. This happens because the gains apply to the subsystem G_2 where the inputs I_1, I_2, F_1 and F_2 yield the output T_1 and T_2. Since the temperatures are unavailable, no direct frequency response identification can be performed and therefore the effects on the bandwidth are not discussed. However, the effects on the performance can be observed from some of the experiments.

The derivative gain stabilizes the response of the actuator at lower frequencies ($f \leq 1$ Hz), but it causes an increase of the delay at higher frequencies. In Figure 4-9, the effects of increasing the derivative gain for the current I_i can be observed. For a derivative gain of $K_{D,I} = 0.25$ the overshoot is clearly present, but for when this gain is increased to 0.5 the overshoot is significantly reduced.

4-2-4 Feed Forward Stabilizer

The graphs in Figure 4-11 shows the experiments that have been performed to identify the stabilizing currents. The experiment consisted of an initial step input which was followed by different values for the stabilizing current. The initial step input drives the output of the actuator to a certain deflection. Then the stabilizer current replaces the initial step input and the output of the actuator can remain constant, which is the

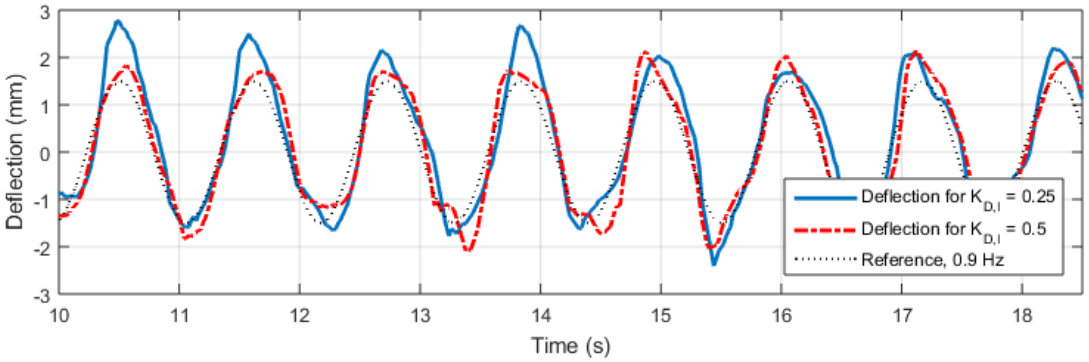

Figure 4-9: Graph depicting the effects of increasing the derivative gain on the error for the current I_i. An increase of the derivative gain from 0.25 to 0.5 significantly reduces the overshoot.

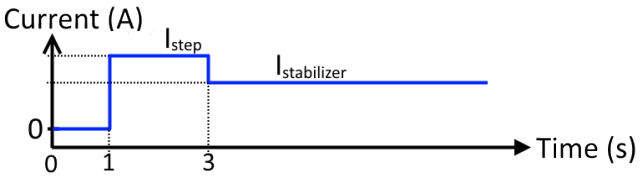

Figure 4-10: Example of the input for the stabilizer current testing. For the time between 1 and 3 seconds the initial step input will drive the output of the system to a certain state. The function of the stabilizer current is to keep the output of the system constant at that state.

desired response, or it can decrease or increase. The response for two different initial currents is depicted in Figure 4-11.

From Figure 4-11 it is clear to see that for certain stabilizing current, the actuator deflection decreases or increases for $t > 3$ seconds. For a number of stabilizing currents, the actuator attains the same deflection, though be it with minor fluctuations. For an initial step input of 1.7 amperes (Figure 4-11a), only the stabilizing current of 1.10 amperes is able to attain a relative constant deflection. For an initial step input of 1.8 amperes (Figure 4-11a), the stabilizing currents 1.15 and 1.20 amperes are both able to maintain a relative constant deflection. The experiment was also done for initial step inputs of 1.4, 1.5 and 1.6 amperes. These experiments combined yielded estimates for the stabilizer current gains I_{FF} and $K_{\text{FF},I}$.

These results seem to indicate that the stress-temperature relation (2-13) for SMA actuators is valid for the SMA-based actuator. This because the deflection rate is equal to zero, the strain rate is also zero. The reason why the deflection is not perfectly constant is assumed to be caused by the erratic temperature behavior. Unfortunately this assumption could not be confirmed since the temperature data was unavailable.

An interesting thing to notice is that deflection of the actuator at $t = 3$ seconds is not always the same for an identical initial step input (Figure 4-11b). This inconsistency

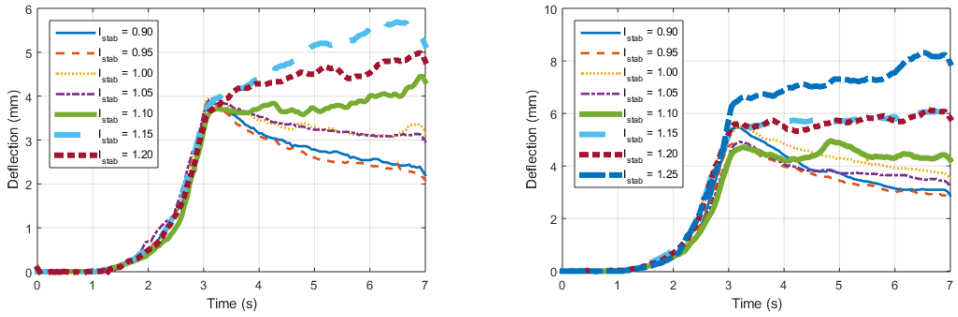

(a) $I_1(1 \leq t \leq 3) = 1.7\ A$ **(b)** $I_1(1 \leq t \leq 3) = 1.8\ A$

Figure 4-11: Actuator response for two different initial currents and different stabilizer currents. The initial step input for $1 \leq t \leq 3$ seconds was **(a)** 1.7 and **(b)** 1.8 amperes, for $t > 3$ seconds the input was equal to the value of the stabilizer currents as defined in the legends of the graphs.

proves to be quite a problem for the tuning of the control parameters. The cause of the inconsistency is thought to be different initial conditions, such as a higher initial temperature from residual heat from previous experiments. The thermal history of the SMA proves to be of significant importance for future experiments. A great effort was made to prevent the lingering of residual heat by venting both valves of the actuator between experiments to bring the temperature of the actuator back to room temperature.

4-3 Control Framework Performance

The results from the individual control principles have all been discussed but an overall performance has yet to be determined. The performance of the general control framework on the SMA-based actuator is based on an analysis on the tracking performance of a single and dual sinusoidal reference over a relevant frequency range and for several amplitudes. Once the performance has been discussed, a short review on the control parameters selection procedure is performed.

4-3-1 Periodical Reference Signal

Several hundred experiments were performed were the actuator was set to follow the reference signal (4-3), where A is the amplitude and B is the frequency in Hz. Figure 4-12 show the response to four different frequencies at the same amplitude. The tracking performance up to a frequency of 1.5 Hz is good, though for increasing frequency the delay slightly increases. The median of the delay for frequencies below 1 Hz is 4 samples, which is equal to a delay of 0.08 seconds. It is uncertain if the delay isn't a result of the limited computational power of the Arduino board, since there was already a problem

with missing samples. The phase delay for the different responses shown in Figure 4-12 are **(a)** 20 degrees, **(b)** 28 degrees, **(c)** 65 degrees and **(d)** 74 degrees.

$$r_i(t) = A\sin(2\pi Bt) \tag{4-3}$$

Inconsistency of the Response

The SMA-based actuator showed an inconsistent response for experiments with identical parameterization and initial conditions. An example of this phenomena is shown in Figure 4-13. Experiment 1 shows a decent tracking performance with a smooth response. The second and third experiment both have some large fluctuations. The cause of the fluctuations for experiment 2 and experiment 3 is unknown. The experiments were executed with a few minutes between them and the valves were vented between experiments to remove any residual heat.

This phenomenon indicates a great challenge in controlling SMA-based actuators, which is the erratic response. This erratic response is thought to be caused by both the erratic temperature response and the non-linear relation between the temperature and the phase transformation rate. The erratic response to a constant current is depicted in the graph in Figure 4-14. It is clear to see that the response is not constant. This could be caused by the erratic temperature response, an unstable current from the power supplies or a non-linear relation between the temperature and the phase transformation rate.

From Figure 4-15 is can be observed that both increasing the frequency as increasing the amplitude of the reference signal increases the mean squared error. Both these parameters influence the required deflection rate. Their influence is expected to be equal. However this is not the case. The graph shows that the influence of the amplitude on the performance is much more dominant than the frequency. At a frequency of 1.2 Hz, the mean squared error for an amplitude of 3.0 millimeters is almost 7 times larger than for an amplitude of 1.0 millimeters. Even the difference between the performance for an amplitude of 2.5 and 3.0 millimeters is a factor 2.

In theory, the required deflection rate for a reference signal with a frequency of 0.5 Hz and an amplitude of 2 millimeter is equal to that for a reference signal with a frequency of 1 Hz and an amplitude of 1 millimeter. The only difference that remains between the required deflection rate is the speed at which they change, that is, the derivative of the deflection rate. Proof for this claim is mathematically expressed by (4-4) and (4-5), where the amplitudes of the two derivatives are equal to each other. This theory suggests that the mean squared error for a reference signal $r_1(t) = \sin(2\pi t)$ should be equal to that of $r_2(t) = 2\sin(\pi t)$, but this is not the case. This leads to the conclusion that the change in deflection rate is not the bottleneck, but that the deflection rate itself is hard to control. This is because the error is significantly larger for reference signals with large amplitudes than reference signals with a low amplitudes (≤ 2 mm) at high frequencies ($f \geq 1$ Hz). The increase of the amplitude of the input signal causes

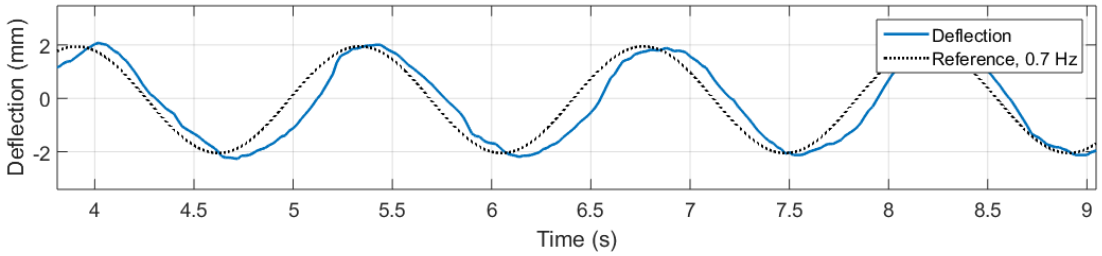

(a) $f_1 = 0.7$ Hz, average delay of 4 samples, $t_d = 0.08$ seconds.

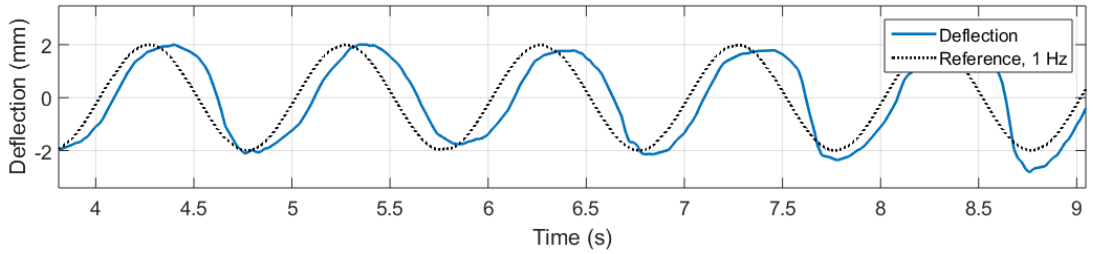

(b) $f_2 = 1$ Hz, average delay of 4 samples, $t_d = 0.08$ seconds.

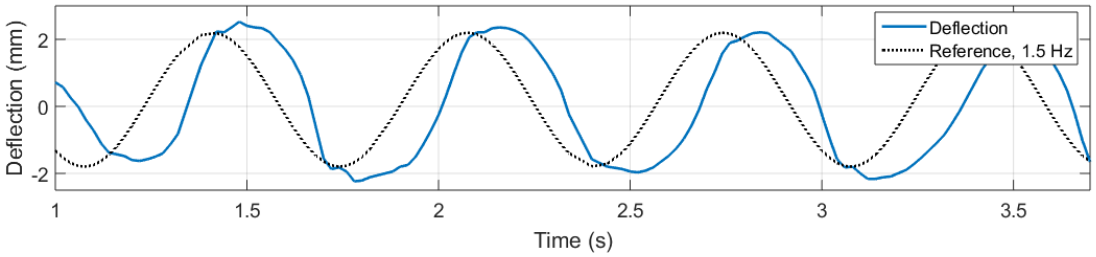

(c) $f_3 = 1.5$ Hz, average delay of 6 samples, $t_d = 0.12$ seconds.

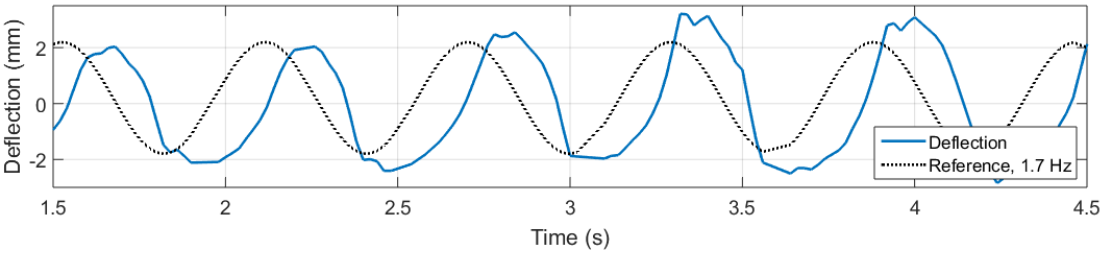

(d) $f_4 = 1.7$ Hz, average delay of 6 samples, $t_d = 0.12$ seconds.

Figure 4-12: Tracking performance for 4 different frequencies and a 2 millimeter amplitude.

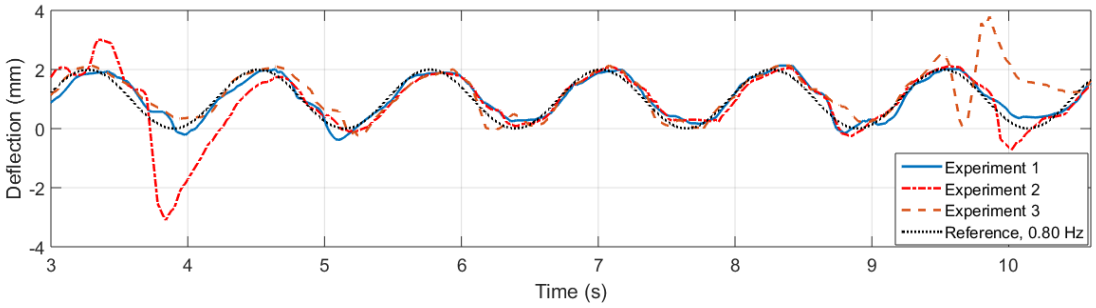

Figure 4-13: Response from three experiments with identical parameterization and initial conditions.

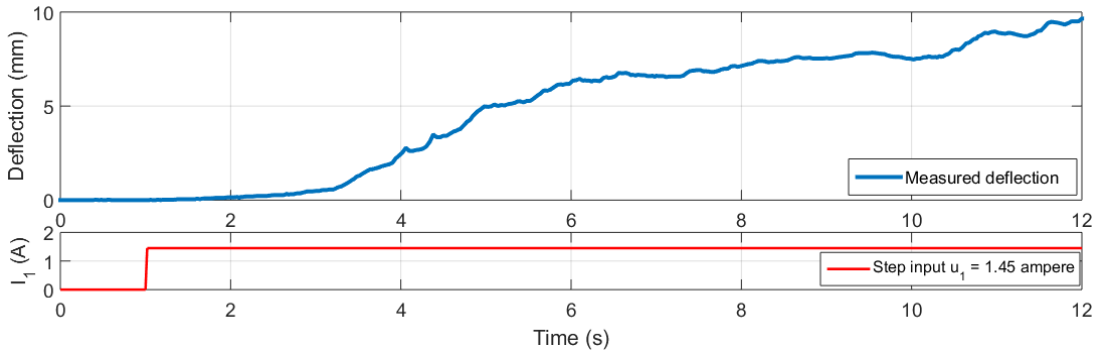

Figure 4-14: Erratic actuator response to a step input with a constant current of $I_1 = 1.45$ ampere which is depicted in the bottom graph.

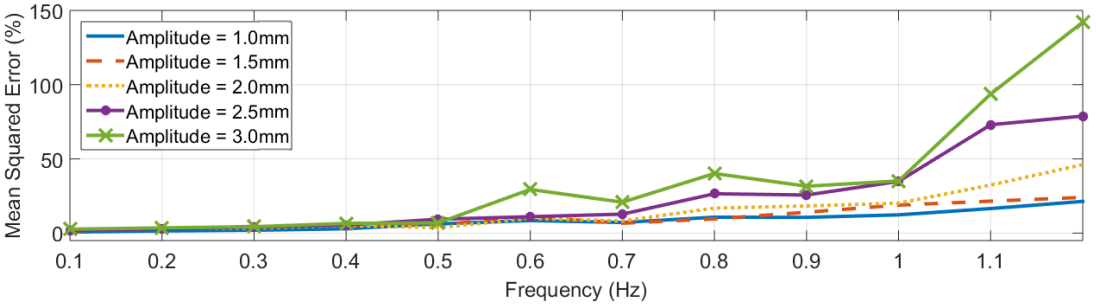

Figure 4-15: Mean squared error of the actuator response for tracking a sinusoidal reference signal with different frequencies and amplitudes.

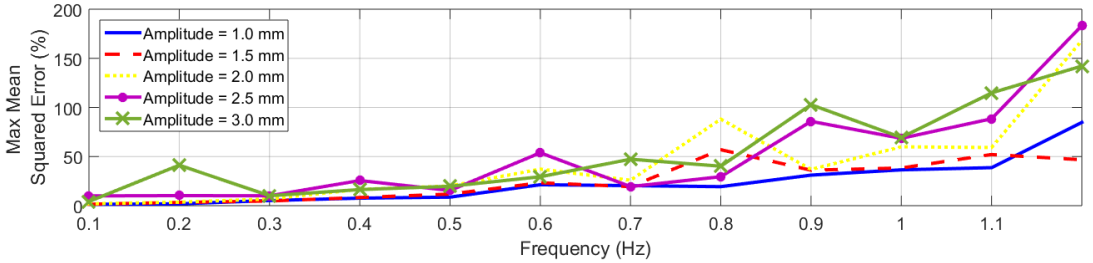

Figure 4-16: Maximum of the mean squared error that were found during the experiments for random parameterization.

so much degradation of the tracking performance that it requires a decrease of the gain values and more damping. This means that the system still has a non-linear response. A frequency response identification would therefore only be valid for inputs with an equal amplitude.

$$\frac{\mathrm{d}}{\mathrm{d}t}\left[A\sin(Bt)\right] = AB\cos(Bt) \tag{4-4}$$

$$\frac{\mathrm{d}}{\mathrm{d}t}\left[\frac{A}{2}\sin(2B\pi t)\right] = AB\cos(2Bt) \tag{4-5}$$

Figure 4-16 shows the mean squared error for the worst combinations of parameter that were encountered during the experiments. These combinations had the highest mean squared error per frequency and amplitude. For frequencies up to 0.5 Hz we can see that the performance is still reasonable. The error for all amplitudes does not exceed 25 %, except for the peak at 0.2 Hz for an amplitude of 3.0 millimeter. Even for bad combinations of parameters the control framework still has a reasonable performance. When the frequency increase this performance really decreases, especially when the amplitude is also increased. This yet again indicates the difficulty of working with a system that still has a non-linear response and an inherently low bandwidth.

Dual Sinusoid

A sinusoidal reference signal was constructed using two sinuses with different frequencies to test the tracking performance for a signal with a average value that is not equal to the neutral position x_0 of the SMA-based actuator. The graph in Figure 4-17 shows the actuator response for a number of different parametrizations. It shows an interesting response to the increase of the derivative gain which seems less damped than for the lower derivative gain (dash-dotted line). By decreasing the proportional gain, the tracking performance increases again (dotted line). The graph shows that the system response destabilizes when the proportional gain is selected too high. It causes a fast switching

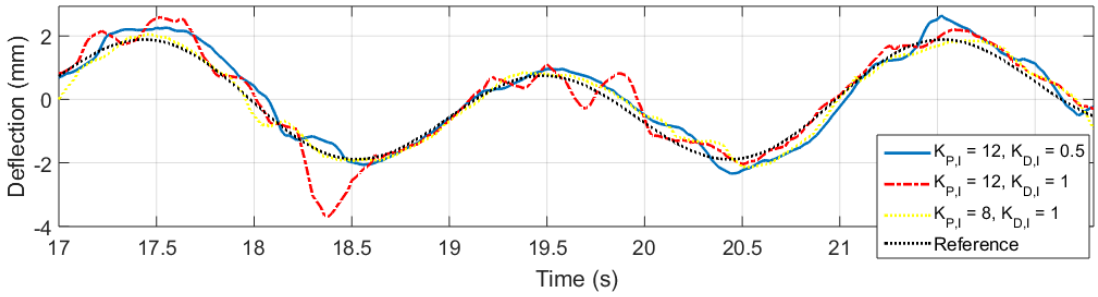

Figure 4-17: Tracking performance of dual sinusoid for different controller parametrizations. Reference signal defined by $r(t) = \sin(\pi t) + \sin(0.5\pi t)$.

and oscillatory response as the controller is unable to maintain a constant deflection. This is especially true in combination with a poor parametrization of the feed forward controller. If the feed forward controller is not able to maintain a constant deflection, the feedback controller is constantly switched on and off. If this controller is overpowered it means that the sign of the error switches very fast.

4-3-2 Non-periodical reference signal

To fully test the performance of the feed forward control law, the response to a step input was tested. The response to a step input determines if the control law is able to maintain a constant deflection once the feedback control law reaches the final reference deflection position. Figure 4-18 shows the response of three experiments with identical parametrization of the controllers to a step input with an amplitude of 1.5 millimeters. The average settling time is approximately 0.5 seconds which is reasonable for SMA-based actuators. The delay from the system is approximately 2 samples, which is equal to 0.04 seconds. This delay is thought to be caused by the hardware of the setup itself and not the SMA-based actuator.

The deflection for $t \geq 2$ seconds is not very smooth, though the average deviation from the set-point is less than 10 %. This inability to maintain a constant deflection can be accredited to two things; either a poorly parametrization of the feed forward controller of the inability of the controller to maintain a constant temperature in the SMA actuators. The latter has already been mentioned and provides a good explaination for the already complicated parametrization of the both the feed forward and feedback control laws. It is impossible to validate the stress-temperature relation of the SMA since temperature data is unavailable and a constant constant temperature of the SMA can therefore not be guaranteed.

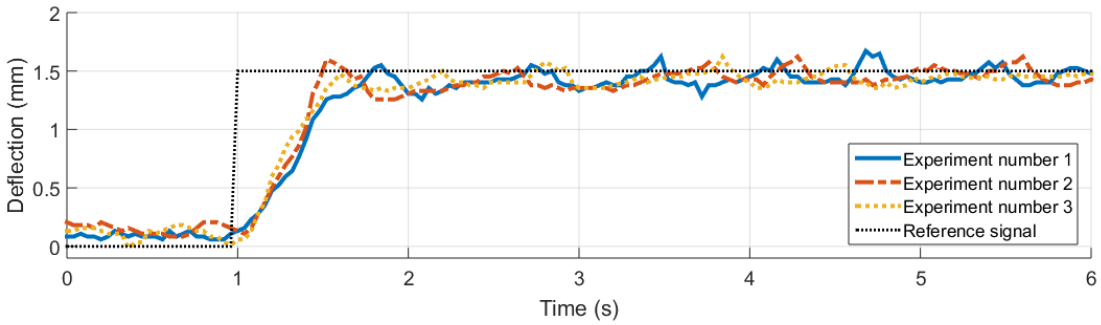

Figure 4-18: Response to a step input as reference for three experiments with identical control parameters.

4-3-3 Parameterization

The control parameters that were used for testing the performance of the general control framework were randomly selected within a certain range. Due to the high number of parameters, there was no possibility to test the performance for each possible combination. Instead, the parameters were intuitively chosen to optimize performance for every specific frequency and amplitude. The expectation was that a pattern would emerge from the measured data.

However, no significant pattern for the selection of control parameters emerged from the measured data. The quality of each parameterization was based on its mean squared error, where a lower error represents a better combination of parameters. The results for the best values for the proportional gain $K_{P,I}$ and for the threshold value for I_i are shown in Table 4-2 and 4-3. There does seem to be a pattern for the proportional gain and the threshold value; the proportional gain seems to decrease for higher frequencies and the threshold value seems to increase for increasing amplitudes. However, since not all combinations of control parameters have been tested it is impossible to determine a real pattern. Listings of the controller parameterizations with the lowest and highest mean squared error can be found in Appendix B.

Bandwidth Filter

During experiments it was also found that the bandwidth filter with one zero and two poles was not optimal. By removing the second pole at the high frequency the performance increased. The second pole resulted in more delay and thus a decrease in performance especially for frequencies higher than 1 Hz.

4-3-4 Influence of Active Cooling

An experiment was designed to investigate the influence of the airflow and sudden valve opening to the excitation of the SMA-based actuator. It was suspected that the sudden

Table 4-2: Best parameter values for the proportional gain $K_{P,I}$ per frequency and amplitude.

Frequency (Hz)	Amplitude (mm) 1.0	1.5	2.0	2.5	3.0
0.1	12	12	12	12	12
0.2	18	8	8	8	8
0.3	18	10	8	10	8
0.4	18	10	12	12	10
0.5	18	12	10	8	10
0.6	18	8	10	8	14
0.7	14	10	10	10	10
0.8	12	10	8	10	14
0.9	12	8	10	8	10
1.0	10	10	14	14	8
1.1	8	8	8	8	8
1.2	8	8	6	8	8

Table 4-3: Best parameter values for the threshold value I_i per frequency and amplitude.

Frequency (Hz)	Amplitude (mm) 1.0	1.5	2.0	2.5	3.0
0.1	1.40	1.40	1.40	1.40	1.40
0.2	1.20	1.40	1.40	1.40	1.40
0.3	1.20	1.50	1.40	1.50	1.50
0.4	1.20	1.25	1.25	1.25	1.25
0.5	1.20	1.40	1.50	1.25	1.50
0.6	1.20	1.25	1.50	1.75	1.00
0.7	1.50	1.25	1.50	1.50	1.50
0.8	1.50	1.25	1.25	1.25	1.00
0.9	1.25	1.50	1.25	1.50	1.50
1.0	1.25	1.50	1.25	1.25	1.50
1.1	1.40	1.25	1.50	1.50	1.50
1.2	1.25	1.25	1.25	1.50	1.50

opening of the valves caused some oscillation which in turn caused an unstable response of the actuator. Figure 4-19 shows the response and corresponding input values of the actuator for one of these experiments. At $t = 2$ seconds, the valve is fully opened, resulting in more oscillations and a deflection of the actuator. The maximum deflection that is caused by the opening of the valves is almost 0.1 millimeters.

The airflow is required to reduce the time required for the Shape Memory Effect (SME) cycle, but there does seem to be a downside of using air to actively cool the SMA actuators. They cause small oscillations which, if they are not filtered properly, can destabilize the system. This is especially true for systems with a high proportional and derivative gain combined with a small delay. The fact that the sudden opening of the

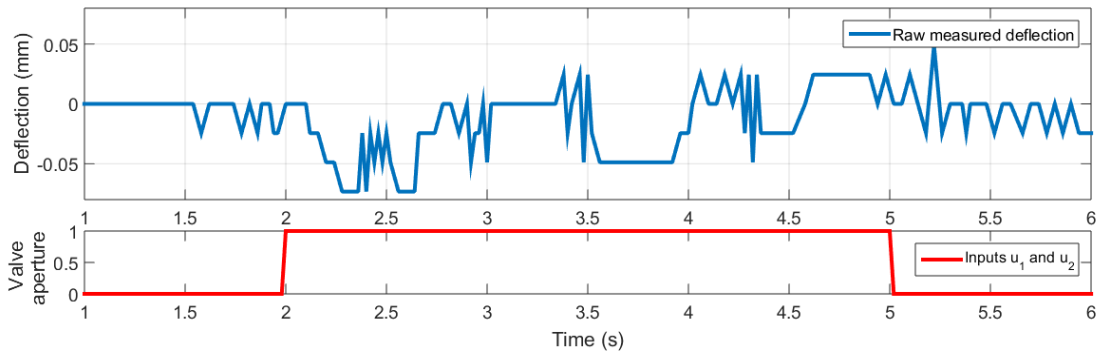

Figure 4-19: Actuator response to sudden opening of the valves showing oscillatory behavior.

valves causes oscillations suggests that it might be beneficial to never fully close the valves and possibly add a low-pass filter to smoothen the control of the valves.

4-3-5 Hardware Performance

It was found, for increasing sampling frequencies, that the data package loss rate increased. This means that for higher sampling frequencies, more samples were lost. For the sampling frequency of 50 Hz an average of approximately 10 percent of the samples was missing. It is unsure however if this is due to the low computational power of the Arduino or that it is purely a communication problem between the Arduino and the PC. However, Windows features a default 125 Hz sampling rate on the USB ports. Therefore it is suspected that the computational power of the Arduino board is too low to facilitate a sufficient sampling rate. However, since the data package loss was not that high, the data could still be used. A simple algorithm was used to calculate the missing samples using linear interpolation.

Another problem that was encountered with the Arduino board was that the voltage of the board dropped by approximately 5% to 10% when the PWM analog outputs were active at a PWM duty cycle of 100 %. When a PWM signal is operating at a duty cycle of 100 % it means that the output is at the maximum voltage. When there is a voltage drop on the Arduino board, the result is that all of the outputs have a lower maximum output voltage. So when a analog output is set to its maximum, which is 5 Volts, it will only go as high as 90 % or 95 % of this value. This means that the accuracy of the control signal drops by the same percentage as the voltage drop.

4-4 Summary

The four control elements of the proposed control framework were individually tested and the results suggests that they had positive effects on the performance of the SMA-based actuator. The control framework was able to solve three of the four challenges that had been posed. The threshold values for the current and the valve aperture ensures that the correct phase transformation is triggered. However, in some cases for certain parametrizations it was found that the combination of the different control elements provided a too aggressive controller output for which it was hard to stop the phase transformations once they had been triggered. This resulted in sharp peaks instead of the smooth peaks from a sinusoidal reference signal.

The challenge that was not solved by the proposed control framework was the non-linear response. The response was found to be close to linear for a certain input range, but that once the input exceeds this range that the response would increase non-linearly. Because the response was still non-linear, the frequency response identification could not be performed since it would only capture the linear dynamics. The linear regime of the input on $e(t)$ was between 0 and 0.3. When the error exceeds this value the response

rapidly increases. This resulted in overshoot for reference signals with a amplitude larger than 2.0 millimeter.

The overall performance of the proposed control framework was good for frequencies below 1 Hz. The response of the actuator still suffers from increasing delay for frequencies exceeding 1.2 Hz. When the amplitude of the reference signal is increased, the performance decreases much faster than for an increase in frequency. This is due to the non-linear response of the SMA-based actuator. For low amplitudes the proposed control framework can achieve good tracking performance even for higher frequencies, though be it with an increase in delay that is proportional to the increase of the frequency.

The combination of the threshold value, the proportional and derivative gain and the feed forward control law sometimes resulted in an overpowered control system which caused some oscillatory behavior. Even with a very large variation of parameters that were tested on the control framework, no significant pattern for the parameterization emerged from all of the experiments. Two important control parameters were analysed for the presence of a pattern for the parameterization. The analysis showed a pattern where the best value for the proportional gain for the current $K_{P,I}$ decreases as the frequency increases and that the best value for the threshold current $I_{\text{threshold}}$ increases as the amplitude increases.

The use of compressed air has led to minor oscillations when the valves are opened. This can potentially destabilize the system and severely decrease the performance if the output signal from the laser is not sufficiently filtered. During the experiments it was found that for each experiment, a number of samples were missing from the data that came from the Arduino. Therefore, the Arduino was deemed to have insufficient computational power to facilitate a constant sample rate. Another undesired phenomenon of the Arduino was a significant voltage drop which was detected when some of the PWM outputs were used at full duty cycle. The drop in voltage results in a loss in accuracy for all outputs of the Arduino board.

Part III

Conclusions and Recommendations

Chapter 5

Conclusions

In this thesis, a general control framework for Shape Memory Alloy (SMA)-based actuators was proposed. The general control framework, or Phase Transformation Approach, uses fundamental properties of the SMA material to construct four control laws. These control laws were specifically designed to solve one of the four challenges that were defined in Chapter 3.

The three questions were formulated in the introduction of the thesis to assess the effectiveness of the control framework will now be answered.

- Can the proposed control framework be parameterized such that it cancels out the hysteretic and non-linear response of the actuator?

  No, the proportional controller that is proposed in the control framework is only able to compensate for the hysteretic response with the correct threshold value. Overall the SMA-based actuator still has a non-linear response. The SMA-based actuator only shows a linear response for a small input range from zero to 0.3 millimeters. So as long as the inputs, and thus the amplitudes of the reference signals, are constrained to this maximum value of the linear regime the control framework will ensure linear operation of the SMA-based actuator. The individual control laws indicate that they are successful in accomplishing their designated objective, although for the linearization objective it is only partly successful. So the general structure and hierarchy of the control framework in their current state are not yet capable of providing linear control of SMA-based actuators, but a with a rearrangement of this hierarchy the linearization may be improved.

- What is the maximal bandwidth that can be achieved with this control framework with a phase delay smaller than 30 degrees?

  The maximal achievable bandwidth is dependent on the amplitude of the input signal. For amplitudes that do not exceed 1.5 millimeters, the bandwidth can go up to approximately 1.5 Hertz. For amplitudes greater than 1.5 millimeters the bandwidth is limited to approximately 1 Hertz.

- What is the influence of different initial conditions of the SMA actuators on its performance?

  The initial conditions such as the temperature and stress are very important for the response of the actuator. If the actuator starts at a higher initial temperature the response is much more aggressive since the transformation temperature is reached faster. A difference in initial stress of the two wires causes an asymmetrical response of the actuator. One of the wires has a lower stress, thus also a lower austenite starting temperature and therefore it reacts faster and more aggressively than the other wire. The fact that there is no real-time information available on the temperature and stress complicates control efforts for the SMA-based actuator.

Discussion

The most challenging issue has been the inconsistent response from the SMA-based actuator. At random times the response would spike or show a really slow response. The real cause for the inconsistent response could not be identified since only one system output was available. If measurements of the temperature or the stress in the SMA wires would have been available, the cause could perhaps have been determined. Some of the fluctuations and inconsistency in the response can possibly be accredited to the different initial conditions. However, since the venting procedures between experiments have been done very consistently, there most likely is another reason for the inconsistent behavior. It is more likely that the erratic behavior is a caused by fluctuation temperatures or the non-linear relation between the phase transformation rate and the temperature.

The practical work was performed on only one of the actuators that was available. This is due to that this actuator is more reliable than the other actuator that had been supplied and that it therefore produces more consistent output data. All SMA wires that have been used were 0.4 millimeter SmartFlex® wires manufactured by SEAS Getters. Unfortunately no tests with alternative SMA wires from other manufacturers have been performed.

Something that was not within the scope of this thesis is the design of the SMA-based actuator. The method for clamping the wires in to the actuator was not optimal. A

constant tension on the SMA wires could therefore not be guaranteed. There was no time for me or my supervisor to improve the design and rebuild the actuator to solve this problem. This is also one of the main reasons why the newer actuator was not used for testing, since for this actuator it was even more difficult to tension the wires. In some of the graphs depicting the response of the actuator it can be observed that the response is not completely symmetrical. This unsymmetrical response was caused by the difference in initial tension in the two SMA wires.

Only a limited amount of parameter combinations have been tested for the proposed control framework. If all combinations had to be tested for reasonable parameter intervals and 5 amplitudes and the 12 frequencies that were now tested, at least 5000 experiments would have had to been performed. This would have taken weeks of brainlessly executing experiments and running optimization scripts. Due to time constraints it was therefore not possible to perform an optimization for the parameteriziation or to identify patterns from the data since the lack of combinations would render them invalid.

Most of the hardware that was used was deemed sufficient. However, the computational capabilities and the internal power regulator of the Arduino board were deemed insufficient. There was a loss of samples and during the experiments, the average voltage of the board sometimes dropped by as much as 10%. This decreases the accuracy and therefore also the reliability of the outputs of the Arduino board.

Recommendations

Throughout this thesis, a number of aspects have been observed that could improve the process of constructing a general control framework for SMA-based actuators. These observations have lead to the following recommendations for future research.

- **Control Framework Structure**
  Some elements of the proposed control framework proved to work for their designated purpose, such as the threshold value and the feed forward stabilizer. However, when some of the elements were combined their controller output often proved too aggressive or out of balance. This suggests a rearrangement of the hierarchy of the control framework. The current hierarchy is that the threshold value, proportional gain and derivative gain are the "main" controller and that the feed forward stabilizer is only active when the main controller is not active. The best threshold values that were found during experiments showed that for an increase in amplitude of the input higher threshold value resulted in better performance. This can be solved by integrating the threshold value and the feed forward stabilizer. The function of the feed forward controller has been to maintain a certain tension in each of the SMA wires. This tension dictates the austenite staring temperature that determines the threshold value. Therefore by integrating these two control elements, the controller ensures that the temperature will approach the austenite

starting temperature. When the temperature is already at the austenite starting temperature, any additional control input causes the stress to increase in the SMA wires causing the actuator to respond. This additional control input can either be achieved by the current proportional and derivative control structure or any other suitable controller. The proportional gain should however be proportional to the amplitude of the input to further linearize the response of the SMA-based actuator. To prevent excitation of the structural modes of the SMA-abased actuator, it is recommended to never fully close the valves and possibly add a low-pass filter to smoothen the control of the valves. This will minimize the oscillations that were observed during the experiments when the valves were suddenly opened and closed.

- **Sensors**
  The absence of measurements of temperature and stress in the SMA wires was really problematic. Therefore it is advised that more effort should be put in embedding one or more sensors in the actuator. An attempt was made to connect a thermocouple to one of the SMA actuators in the SMA-based actuator. However, a thermocouple has to be welded on to the surface of the material of which it has to measure the temperature. This presents a huge problem for a SMA wire which only has a diameter of 0.4 millimeters, which is approximately the same diameter of the wires of the thermocouple itself. Real time data of the temperatures and/or stress of the SMA wires allows for better control using the models that have been discussed. A better analysis of the cause of the fluctuations is then also possible.

- **I/O interface**
  The input and output interface and the all the computational work should not be processed by an Arduino board. It is recommended that a more powerful system is used to improve both the accuracy of the controller outputs but also to improve the reliability of the data acquisition.

- **Clamping mechanism**
  A better clamping mechanism is required to ensure a constant tension and also the possibility of fine tuning of the tension. During the experiments, some asymmetrical behavior was noticed which can only be caused by a difference in initial tension in the SMA wires. A better clamping mechanism ensures a smoother and more consistent response of the SMA-based actuator.

- **Modeling**
  If there is no possibility of obtaining more sensory information such as the temperature or the stress, another option would be to construct a more detailed model that describes the mechanics of the actuator. If the deflection can be expressed as a function of the stress, this stress can then possibly be coupled to a certain input. It would still be very complicated to incorporate the influences of the valve aperture in this approach.

Part IV

Appendix

Appendix A

Hardware

A-1 SMA-based Actuator

The Shape Memory Alloy (SMA)-based actuator that was used for this thesis was designed an manufactured by Adrian Lara-Quintanilla [4]. The actuator is shown in Figure A-1.

SMA-actuator

The SMA actuator that were used in the SMA-based actuator were from the SmartFlex® which are manufactured by SEAS Gettter. The properties of the wire are shown in Table A-1.

Figure A-1: Picture of the actuator with the connections indicated. The base indicates where the actuator is clamped into the setup and the tip of the actuator is where the deflection is measured.

Table A-1: SMA wire properties

	Diameter	Density	Specific Heat Capacity[1]
SmartFlex®	400 μm	6450 $^{kg}/_{m^3}$	700 $^{J}/_{kgK}$

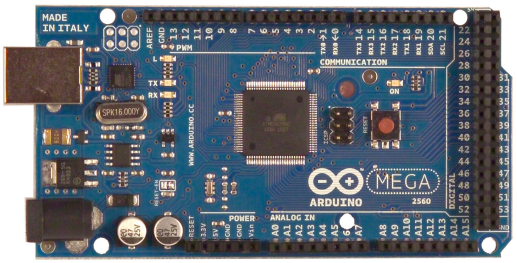

Figure A-2: An Arduino Mega 2560 board.

A-2 Setup

The illustration in Figure A-3 depicts the configuration of the used hardware and the connections between them. The device that facilitated the input and output interface and also runs the control framework was a board from Arduino. The Arduino Mega 2560 had been selected because it offers standalone operation and real-time tuning and monitoring in the Simulink.

Arduino Mega 2560

A picture of the type of Arduino that was used is shown in Figure A-2. The relevant specifications of the Arduino board that was used are listed in Table A-2. The Arduino was connected via USB and was power both by USB and an external power supply at 12 volts and 2 ampere. The internal power regulator automatically selects the best suitable power source.

Displacement sensor

The displacement sensor that was used was the optoNCDT 1401 from Micro-Epsilon (Figure A-4). The laser sensor has a range of 20 millimeters. The laser sends an analog output signal, where 1 volt corresponds to the beginning of the range at a distance of 30 millimeter and 5 volts corresponds to the end of the measurement range at a distance of 50 millimeters. The sensor has a minimal resolution of 5 micrometer.

Table A-2: Relevant specifications of the Arduino Mega 2560

Clock speed:	16 MHz
SRAM:	8 KB
Flash memory:	256 KB (248 KB available)
Digital I/O:	54 (of which 15 provide PWM output)
DC current per pin:	40 mA
Analog Inputs:	16
Resolution Analog Inputs:	10 bits
Voltage Resolution Analog Inputs:	≈ 5 millivolt
Special:	Standalone Matlab and Simulink execution Interactive tuning and monitoring

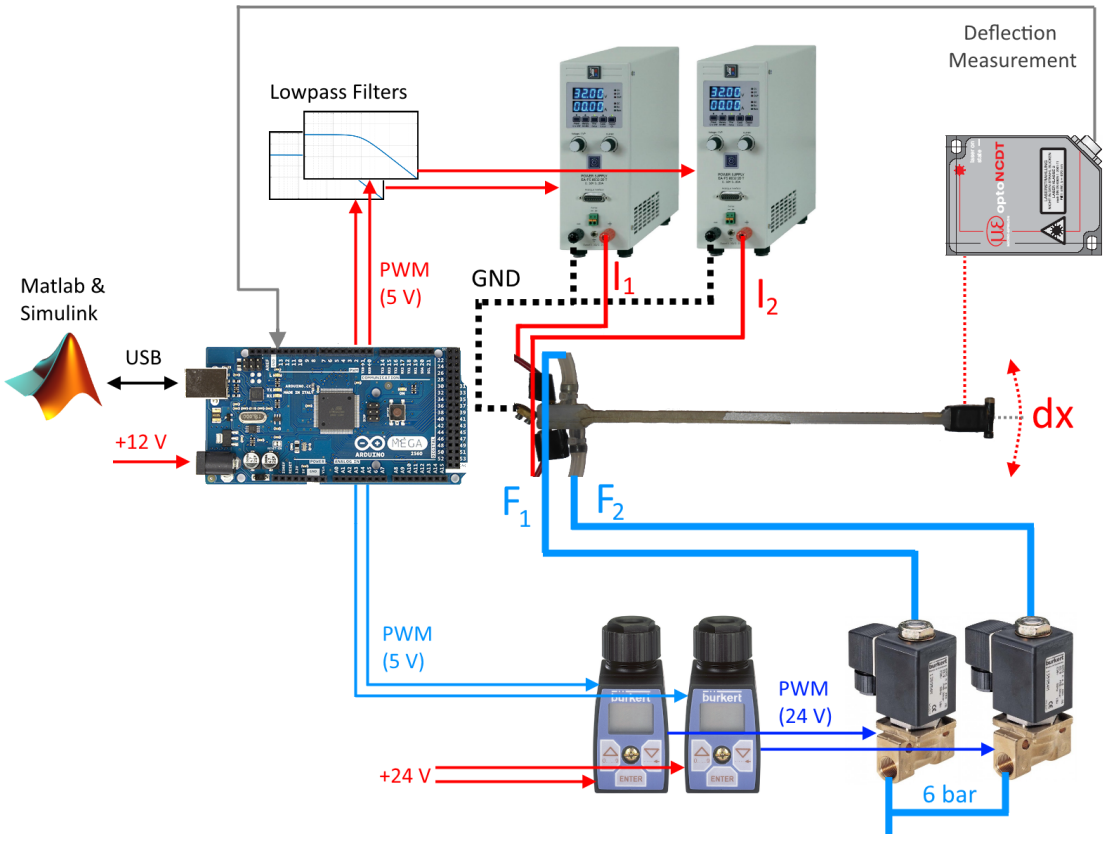

Figure A-3: Illustration depicting the total hardware setup and connections.

Figure A-4: Mirco-Epsilon optoNCDT 1401 laser displacement sensor.

PWM Low-Pass Filters

An analog low pass filter was used for the Pulse Width Modulation (PWM) outputs of the Arduino to the analog inputs of the power supplies. A resistor of 2.4 $K\Omega$ and a capacitor of 3.3 μF were used to build the analog low pass filter. The theoretical response of the filter is shown in Figure A-5.

Power Supply Power Relay

During early experiments the Arduino board had some problems with initializing the code from Simulink. During the initialization it would reset the analog outputs but this sometimes resulted in very high outputs on these ports. For a few experiments this resulted in an output from the power supply of over 10 ampere. It caused the wire to heat up beyond the melting temperature of the nylon of the actuator, which caused the SMA wires to melt into the nylon. To prevent this from occurring, a simple power relay was constructed. The relay was set remotely operate the power supplies, setting it to standby by default and to "on" for when Simulink was done with the compiling and the Arduino was done with the initialization.

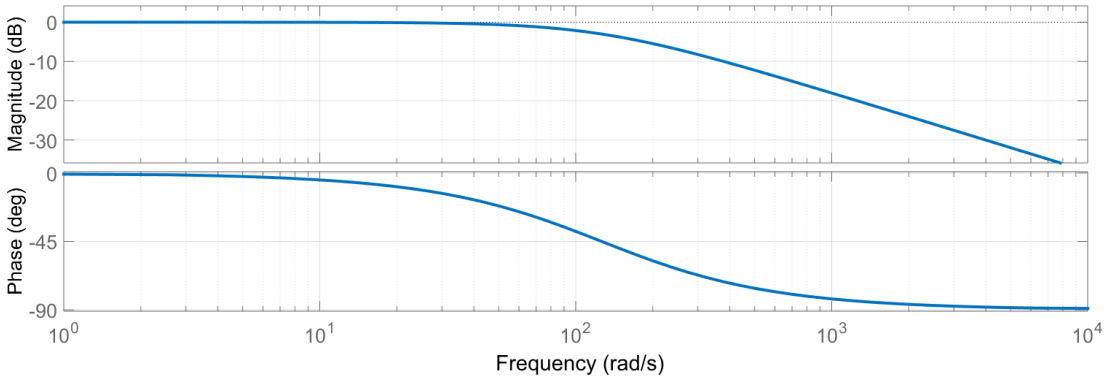

Figure A-5: Bode plot estimate for the analog low pass filter.

Table A-3: Specifications of the Elektra-Automatik model EA-PS 8032-20

Output Current:	0-20 A
Output Voltage:	0-32 V
Output Power:	640 W
Regulation (10-100 % load):	$<$ 2 ms
Stability (0-100% load):	$<$ 0.15%

A-3 Power Supplies

Two power supplies from Elektra-Automatik were used to supply the current to the two SMA wires in the SMA-based actuator (Figure A-6). The specifications for the model EA-PS 8032-20 are listed in Table A-3.

A-4 Valves

For the airflow control, two proportional valves (Type 2821) from Burkert were used (Figure A-7a). The valves were rated to a maximum pressure of 6 bar. The valves were controlled by valve controllers (Type 8605) from Burkert (A-7b). A power supply from National Instruments (FP-PS-4) was used to power the valve controllers. The FieldPoint power supplies delivers +24 volts to both valve controllers.

Figure A-6: Elektra-Automatik EA-PS 8032-20.

(a) **(b)**

Figure A-7: Proportional valve **(a)** and a valve controller **(b)** from Burkert.

Appendix B

Control Framework Parameters

This appendix list the control parameters that were found to have the lowest mean squared error per frequency and amplitude of a sinusoidal reference signal. The mean squared error is calculated with Equation B-1, where n is the number of samples of the output $y(k)$ and reference signal $r(k)$.

$$\text{MSE} = \frac{1}{n}\sum_{i=1}^{n}(y(k) - r(k))^2 \tag{B-1}$$

Table B-1: Best parameter values for the threshold value for the current I_i per frequency and amplitude.

Frequency	Amplitude (mm)				
(Hz)	1.0	1.5	2.0	2.5	3.0
0.1	1.40	1.40	1.40	1.40	1.40
0.2	1.20	1.40	1.40	1.40	1.40
0.3	1.20	1.50	1.40	1.50	1.50
0.4	1.20	1.25	1.25	1.25	1.25
0.5	1.20	1.40	1.50	1.25	1.50
0.6	1.20	1.25	1.50	1.75	1.00
0.7	1.50	1.25	1.50	1.50	1.50
0.8	1.50	1.25	1.25	1.25	1.00
0.9	1.25	1.50	1.25	1.50	1.50
1.0	1.25	1.50	1.25	1.25	1.50
1.1	1.40	1.25	1.50	1.50	1.50
1.2	1.25	1.25	1.25	1.50	1.50

Table B-2: Best parameter values for the threshold value for the valve aperture F_i per frequency and amplitude.

Frequency	Amplitude (mm)				
(Hz)	1.0	1.5	2.0	2.5	3.0
0.1	0.50	0.50	0.50	0.50	0.50
0.2	0.35	0.50	0.50	0.50	0.50
0.3	0.35	0.50	0.50	0.50	0.50
0.4	0.35	0.50	0.50	0.50	0.50
0.5	0.50	0.50	0.75	0.50	0.75
0.6	0.50	0.50	0.75	0.75	0.60
0.7	0.75	0.40	0.50	0.50	0.50
0.8	0.75	0.50	0.50	0.50	0.60
0.9	0.50	0.50	0.50	0.50	0.50
1.0	0.50	0.50	0.50	0.50	0.75
1.1	0.50	0.25	0.50	0.50	0.50
1.2	0.25	0.25	0.25	0.50	0.50

Table B-3: Best parameter values for the proportional gain $K_{P,I}$ per frequency and amplitude.

Frequency	Amplitude (mm)				
(Hz)	1.0	1.5	2.0	2.5	3.0
0.1	12	12	12	12	12
0.2	18	8	8	8	8
0.3	18	10	8	10	8
0.4	18	10	12	12	10
0.5	18	12	10	8	10
0.6	18	8	10	8	14
0.7	14	10	10	10	10
0.8	12	10	8	10	14
0.9	12	8	10	8	10
1.0	10	10	14	14	8
1.1	8	8	8	8	8
1.2	8	8	6	8	8

Table B-4: Best parameter values for the proportional gain $K_{P,F}$ per frequency and amplitude.

Frequency	Amplitude (mm)				
(Hz)	1.0	1.5	2.0	2.5	3.0
0.1	0.50	0.50	0.50	0.50	0
0.2	2.00	0	0	0	0
0.3	2.00	0	0	0.25	0
0.4	2.00	0	0.25	0.50	0
0.5	1.00	0.25	2.00	1.00	4.00
0.6	1.00	1.00	2.00	4.00	1.00
0.7	4.00	0.50	0.50	0.50	0.50
0.8	4.00	1.00	1.00	1.00	1.00
0.9	0.50	4.00	0.50	4.00	4.00
1.0	1.00	0.50	2.00	2.00	4.00
1.1	0.50	0.50	0.50	0.50	0.50
1.2	0.50	0.50	0.50	0.50	0.50

Table B-5: Best parameter values for the derivative gain $K_{D,I}$ per frequency and amplitude.

Frequency	Amplitude (mm)				
(Hz)	1.0	1.5	2.0	2.5	3.0
0.1	1.50	1.00	1.00	1.00	1.0000
0.2	0.20	0.75	0.75	1.00	1.50
0.3	0.20	1.00	0.75	1.00	1.00
0.4	0.15	1.00	1.00	1.00	1.00
0.5	0.50	0.50	1.50	1.25	1.00
0.6	0.50	0.25	1.50	1.25	0.30
0.7	1.50	1.50	0.50	0.50	0.50
0.8	1.50	1.25	1.25	1.25	0.30
0.9	0.20	1.25	1.50	1.25	0.25
1.0	0.25	0.50	1.50	1.25	1.00
1.1	1.00	0.75	0.50	0.50	0.50
1.2	1.00	1.25	1.25	0.50	0.50

Table B-6: Best parameter values for the derivative gain $K_{D,F}$ per frequency and amplitude.

Frequency	Amplitude (mm)				
(Hz)	1.0	1.5	2.0	2.5	3.0
0.1	1.50	1.00	1.00	1.00	1.0000
0.2	0.20	0.75	0.75	1.00	1.50
0.3	0.20	1.00	0.75	1.00	1.00
0.4	0.15	1.00	1.00	1.00	1.00
0.5	0.50	0.50	1.50	1.25	1.00
0.6	0.50	0.25	1.50	1.25	0.30
0.7	1.50	1.50	0.50	0.50	0.50
0.8	1.50	1.25	1.25	1.25	0.30
0.9	0.20	1.25	1.50	1.25	0.25
1.0	0.25	0.50	1.50	1.25	1.00
1.1	1.00	0.75	0.50	0.50	0.50
1.2	1.00	1.25	1.25	0.50	0.50

Table B-7: Best parameter values for the stabilizer current I_{FF} per frequency and amplitude.

Frequency	Amplitude (mm)				
(Hz)	1.0	1.5	2.0	2.5	3.0
0.1	1.00	1.00	1.00	1.00	0
0.2	1.00	1.00	1.00	1.10	0
0.3	1.00	0	1.00	0	0
0.4	1.00	0	0	0	0
0.5	1.10	1.00	0.80	0	1.00
0.6	1.10	0.80	0.80	0.80	0.80
0.7	0.80	0	0.80	0.80	0.80
0.8	0.80	0	0	0	0.80
0.9	0.80	0.25	0	0.25	0.25
1.0	0.80	0.80	0.25	0.25	1.00
1.1	1.00	0	0.80	0.70	0.70
1.2	0	0	0	0.70	0.70

Table B-8: Best parameter values for the proportional gain K_{FF} for the stabilizer current I_{FF} per frequency and amplitude.

Frequency	Amplitude (mm)				
(Hz)	1.0	1.5	2.0	2.5	3.0
0.1	2.50	2.50	2.50	2.50	0
0.2	0.75	2.50	2.50	2.00	0
0.3	0.75	0	2.50	0	0
0.4	0.75	0	0	0	0
0.5	0.60	2.50	0.25	0	0.50
0.6	0.60	0.50	0.25	0.25	0.50
0.7	0.50	0	1.50	1.50	1.00
0.8	0.50	0	0	0	0.50
0.9	0.50	0	0	0	0.25
1.0	0.50	2.00	0.25	0.25	0.50
1.1	2.00	0	2.00	2.00	2.00
1.2	0	0	0	2.50	2.50

Bibliography

[1] J. Kudva, "Overview of the darpa smart wing project." *Journal of Intelligent Material Systems and Structures*, vol. 15, pp. 261–267, 2004.

[2] T. Barlas and G. van Kuik, "Review of state of the art in smart rotor control research for wind turbines," *Progress in Aerospace Sciences*, vol. 46, pp. 1–27, 2010.

[3] ——, "State of the art and prospectives of the smart rotor control for wind turbines," *Journal of Physics*, 2007.

[4] A. Lara-Quintanilla, A. W. Hulskamp, and H. E. Bersee, "A high-rate shape memory alloy actuator for aerodynamic load control on wind turbines," *Journal of Intelligent Material Systems and Structures*, vol. 24, no. 15, pp. 1834–1845, 2013.

[5] T. Koomen, *Control of Shape Memory Alloy Based Actuators: A Review on Control Strategies and the Potential of a General Framework*, Delft University of Technology Std., November 2014.

[6] R. Stalmans and J. Van Humbeeck, "Shape memory alloys: Functional and smart," in *Smart Materials and Technologies - sensors, control systems and regulators*, 1995.

[7] D. C. Lagoudas, *Shape Memory Alloys - Modeling and Engineering Applications*. Springer.

[8] J. H. Crews and G. D. Buckner, "Design optimization of a shape memory alloy-actuated robotic catheter," *Journal of Intelligent Material Systems and Structures*, vol. 23, no. 5, pp. 545–562, 2012b.

[9] M. K. Stanford, "Thermophysical properties of 60-nitinol for mechanical component applications," *National Aeronautics and Space Administration*, 2012.

[10] S. Getters, "Smartflex wire," SAES Getters, Tech. Rep., 2009.

[11] L. Brinson, "One-dimensional constitutive behavior of shape memory alloys: Thermomechanical derivation with non-constant material functions and redefined martensite internal variable," *Journal of Intelligent Material Systems and Structures*, vol. 4, no. 2, pp. 229–242, 1993. [Online]. Available: http://jim.sagepub.com/content/4/2/229.abstract

[12] S. Seelecke, "Modeling the dynamic behavior of shape memory alloys," *International Journal of Non-Linear Mechanics*, vol. 37, no. 8, pp. 1363 – 1374, 2002. [Online]. Available: http://www.sciencedirect.com/science/article/pii/S0020746202000306

[13] S. Seleecke and I. Müller, "Shape memory alloy actuators in smart structures: Modeling and simulation," *Applied Mechanics Reviews*, vol. 57, no. 1, pp. –, 2004.

[14] O. Heintze, "A computationally efficient free energy model for shape memory alloys - experiments and theory," Phd, 2004.

[15] K. Arai, K. Aramaki, and K. Yanagisawa, "Continuous system modelling of shape memory alloy (sma) for control analysis," 1994.

[16] W. Wang and S. Yan, "A new continuous model of shape memory alloys," *Applied Mechanics and Materials*, vol. 226-228, pp. 2467–2470, 2012.

[17] A. Nespoli, S. Besseghini, S. Pittaccio, E. Villa, and S. Viscuso, "The high potential of shape memory alloys in developing miniature mechanical devices: A review on shape memory alloy mini-actuators," *Sensors and Actuators A: Physical*, vol. 158, no. 1, pp. 149–160, 2010.

[18] K. Ikuta, M. Tsukumoto, and S. Hirose, "Shape memory alloy servo acttuator system with electric resistance feedback and application for active endoscope," 1988.

[19] L. Toia, A. Coda, G. Vergani, and A. Mangioni, "Functional characterization of sma wires in actuation conditions," SEAS Getters, Tech. Rep.

[20] D. J. Hartl and D. C. Lagoudas, "Aerospace applications of shape memory alloys," *Proceedings of the Institution of Mechanical Engineers, Part G: Journal of Aerospace Engineering*, vol. 221, no. 4, pp. 535–552, 2007. [Online]. Available: http://pig.sagepub.com/content/221/4/535.abstract

[21] A. Lara-Quintanilla and H. Bersee, "Improvement of the attainable working frequency of sma wires by means of active cooling and working strain-ratios," *ASME 2014 Conference on Smart Materials, Adaptive Structures and Intelligent Systems*, 2014.

[22] G. Song and N. Ma, "Robust control of a shape memory alloy wire actuated flap," *Smart Materials and Structures*, vol. 16, no. 6, pp. N51–N57, 2007.

[23] C. Bil, K. Massey, and E. J. Abdullah, "Wing morphing control with shape memory alloy actuators," *Journal of Intelligent Material Systems and Structures*, vol. 24, no. 7, pp. 879–898, 2013.

[24] F. Peng, X.-X. Jiang, Y.-R. Hu, and A. Ng, "Actuation precision control of sma actuators used for shape control of inflatable sar antenna," *Acta Astronautica*, vol. 63, no. 5-6, pp. 578–585, 2008.

[25] A. Lara-Quintanilla, "Manufacturing and control of shape memory alloy based actuators," Master Thesis, 2010.

[26] G. S. Batur, V. Chaudhry, and C., "Precision tracking control of shape memory alloy actuators using neural networks and a sliding-mode based robust controller," *Smart Materials and Structures*, vol. 12, no. 2, p. 223, 2003.

[27] K. J. Aström and B. Wittenmark, *Computer Controlled Systems. Theory and Design*, T. Kailath, Ed. Prentice Hall, 1997, page 244.

Glossary

List of Acronyms

3mE	Mechanical, Maritime and Materials Engineering
AE	Aerospace Engineering
DCSC	Delft Center for Systems and Control
MISO	Multi Input, Single Output
PWM	Pulse Width Modulation
SISO	Single Input, Single Output
SMA	Shape Memory Alloy
SMC	Sliding Mode Control
SME	Shape Memory Effect
DCSC	Delft Center for Systems and Control
ETFE	Empirical Transfer Function Estimate
FF	Feed Forward
ILC	Iterative Learning Controller
NN	Neural Networks
PID	Proportional, Integral and Derivative
PD	Proportional and Derivative
RBS	Random Binary Signal